Polarizable Embedding Approach for the Analytical Calculation of Raman and Raman Optical Activity Spectra of Solvated Systems

Tommaso Giovannini,[†] Marta Olszòwka,[†] Franco Egidi,[†] James R. Cheeseman,[‡] Giovanni Scalmani,[‡] and Chiara Cappelli[*,†]

†*Scuola Normale Superiore, Piazza dei Cavalieri 7, 56126 Pisa, Italy*

‡*Gaussian Inc. 340 Quinnipiac St Bldg 40, Wallingford, CT 06492, USA*

E-mail: chiara.cappelli@sns.it

Abstract

We present an analytical formulation and implementation of Raman and Raman Optical Activity (ROA) spectra within a three-layer fully polarizable Quantum Mechanical (QM)/ Molecular Mechanics (MM)/Polarizable Continuum Model (PCM) approach. Polarization effects in the MM layer are modeled by exploiting the Fluctuating Charges (FQ) method, in which MM solvent atoms are endowed with electric charges that can be mutually polarized by the solute QM density. Because of its fully polarizable atomistic description, QM/FQ/PCM is able to account for specific solvent effects like those due to hydrogen bonds, providing a physical picture for protic solvents such as water. Applications to aqueous (R)-methyloxirane and (S)-methyllactate are presented, and results are compared with available experimental data.

1 Introduction

Multiscale modeling, based both on implicit, explicit, or mixed explicit-implicit approaches has demonstrated to be a powerful methodology to account for environmental effects on the calculation of many spectral signals.[1–8] In this respect, the most successful approaches fall within the class of the so-called 'focused models", in which the attention is focused on the properties of a target molecule (the solute in case of solutions), which are modified, but not determined, by the presence of the surrounding environment (the solvent). Focused models rely on a partition of the molecular system, in which the various regions are treated at a different level of accuracy. In general, the target is accurately modeled, by resorting to Quantum Mechanical (QM) methods, whereas the environment is treated at a lower level, generally by resorting to classical approaches.

The goal of focused models is to accurately reproduce both the properties of the target and its interactions with the environment, while the properties of the latter are of secondary importance and may not computed. Thanks to this paradigm, such models do not significantly increase the cost of a QM calculation with respect to the isolated system, which is a feature that has contributed to their popularity. Among the focused models that have been proposed to account for environmental effects on spectroscopic and response properties, one of the most used is the Polarizable Continuum Model (PCM).[1] There are, however, cases when the electrostatic interaction described by a continuum is not enough, such as cases where hydrogen bonds can form between solute and solvent.[9]

One way to address this problem is to restore the atomistic detail in the description of the solvent, which can be modeled classically by means of molecular mechanics (MM),[2,10–15] and QM/MM methods have in fact been used in the past to model Raman and ROA spectra of molecules in solution.[3,5,16–18] Contrary to what happens in PCM, however, in standard MM force-fields there is no mutual polarization between the solute and the solvent since the parameters defining the latter are fixed, therefore the solvation interaction does not directly affect the spectroscopic response. Mutual polarization, however, can be restored by employ-

ing a polarizable force-field, based on distributed multipoles,[19–21] induced dipoles,[22–24] Drude oscillators[25] or Fluctuating Charges (FQ),[26,27] which is exploited in this study. This model, and its three-layer extension QM/FQ/PCM where a polarizable continuum surrounds the system to model bulk solvent properties, have been successfully employed for the calculation of a variety of molecular properties for systems in aqueous solution,[8] including those related to the study of chiral systems, such as Electronic Circular Dichroism,[28] Vibrational Circular Dichroism,[29] and Optical Rotation.[9,30,31]

Another spectroscopic technique which in the last decades has demonstrated its power for the investigation of chiral compounds is Raman optical activity (ROA), which was first genuinely measured by Barron and Buckingham.[32–34] ROA can be defined as the difference in intensity of the Raman scattered radiation for right and left circularly polarized light, which can be positive or negative depending on the absolute configuration of the sample. As a mixed electronic-vibrational techniques, a ROA spectrum carries structural information about a sample, much like VCD, however it is also blessed by the same advantages possessed by Raman spectroscopy over Infrared (IR) absorption spectroscopy, such as the possibility of more easily recording spectra of analytes in aqueous solution.

A problem shared by all such techniques, when they are used to assign the absolute configuration of a sample, is that the exact correspondence between a positive or negative spectroscopic response to each enantiomer is not known, therefore the assignment must rely on other data, such as the result of quantum chemical calculations, which can provide an unambiguous way to interpret the experimental measurements. This is the reason why much effort has been devoted over the years to the development of accurate and efficient computational techniques that provide calculated results that are directly comparable to experiment.[35]

The first numerical ab initio ROA calculations were reported in 1990 by Polavarapu[36] using the static-limit approximation[37] and magnetic field independent basis functions. Further developments of the theoretical approach include the extension to frequency-dependent Density Functional Theory (DFT) response,[38,39] the development of fully analytical third derivative

methods of the Hartree-Fock wave function,[40,41] the use of Gauge Including Atomic Orbitals[42,43] (GIAO) which ensure the results are independent of the gauge origin.[44–47]

All such developments were instrumental in making the calculation of ROA spectra available to both expert theoreticians and experimentalists however, though the ability to perform a simulation based on some choice of electronic structure theory model or DFT functional is necessary, it is often not enough to obtain results that can be directly compared to experiment. A major issue that has to be addressed is the fact that most experiments are performed on samples in the condensed phase, particularly on neat liquids or solutions.

In fact, the presence of a solvent may drastically affect the sign of the measured property,[9,48–50] therefore it is crucial to employ models that take these effects into account. To address these issues, we present for the first time a fully analytical implementation of Raman and ROA intensities calculation for molecules both in the gas phase and in solution by exploiting the polarizable QM/FQ/PCM model, based on Time-Dependent Density Functional Theory (TDDFT).

From the theoretical point of view, ROA can be described as a third-order property, in which three types of perturbations must be considered at the same time, i.e. electric, magnetic, vibrational.[36,51] While the ROA tensors are usually expressed in a sum-over-state fashion,[52] in the far-from-resonance (FFR) regime, i.e. when the frequency laser radiation that stimulate the ROA response is far removed from any electronic absorption band of the sample, the ROA intensity can then be described in terms of geometrical derivatives of the system's polarizability tensors. Therefore, in order to extend the QM/FQ/PCM model to the analytical calculation of all the necessary third order properties defining such spectra, the FQ and PCM interaction terms in the Hamiltonian propagate in the derivation of response properties of arbitrary order, resulting in the presence of additional terms in the response functions. The formulation which is here presented lays its foundations on the focused model paradigm, i.e. only the solute vibrations are considered, thus no geometrical derivatives of the energy with respect to the position of the MM atoms need to be evaluated.

The paper is organized as follows: after a brief section recalling the basics of the QM/FQ/PCM approach, the analytical formulation of the polarizability tensors' derivatives occurring in ROA is presented for isolated molecules. Next, all the explicit QM/FQ/PCM contributions are derived. They are followed by the presentation of test applications on aqueous solutions of (R)-methyloxirane and (S)-methyllactate , for which the computed spectra are also compared with available experimental data. Finally, the main points are summarized and some future perspectives are proposed.

2 Theory

2.1 QM/FQ/PCM model

In the FQ model, each MM atom is endowed with a charge that is not fixed, but varies because it interacts with the electrostatic potential generated by the solute. The fluctuating charges of the MM layer can thus respond to both the electrostatic potential generated by the solute and the solvent reaction field, while the solute feels the presence of the FQs and the solvent through specific terms that appear in the QM Hamiltonian. The solvent reaction field is consistent with the electrostatic potential generated by both the solute's electronic density and the fluctuating charges. For spectroscopic properties, such interaction terms also propagate to the solute's response equations.[53–55] The three-layer QM/FQ/PCM approach falls within the family of focused models, where the properties of the classical layers are not considered crucial, and the modeling of the solvent, from the physics behind mathematical treatment to the parametrization, are developed in a way that best reproduces its effect upon the solute. Thus, when calculating a spectrum, the response arises from the quantum-mechanical solute alone, though the solvent can still significantly affect it through specific interaction terms that appear in the Hamiltonian.

In figure 1 the three layers are schematically presented. The solute, described using a QM method, is at the center of a spherical region containing a number of solvent molecules,

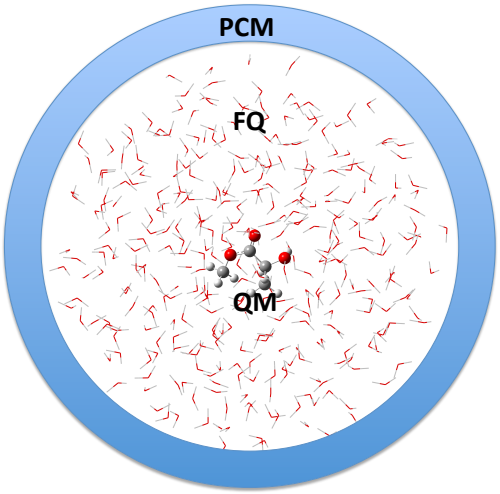

Figure 1. Schematic representation of the QM/FQ/PCM model.

which are described classically and whose atoms carry fluctuating charges that can respond to the solute's electrostatic potential. The size of this region, and thus the number of explicit solvent molecules to be included, is chosen to make sure all specific solute-solvent interactions are taken into account, and their positions are taken from a classical molecular dynamics (MD) simulation which samples the solute-solvent configuration space. At the boundary of the FQ region we find the surface of a polarizable continuum which is used to model bulk solvent effects and to introduce proper non-periodic boundary conditions. Notice that in principle a shape other than spherical (e.g. an ellipsoid) could be chosen as boundary for prolate molecular systems.

The FQ approach[29,56] is especially suitable for the evaluation of spectroscopic properties in a polarizable QM/MM framework because, as shown below, it yields an energy expression that is easily differentiable allowing the calculation of response properties of high order. The model is based on a set of parameters representing atomic hardnesses and electronegativities, whose physical origin can be rigorously defined within the so called "conceptual DFT".[57,58] Through these parameters, atomic charges can be computed depending on the solute electrostatic potential.[26,27] More in detail, the FQ approach describes the polarization effects by endowing each MM atom with a fluctuating charge, whose value depends on the electrostatic potential[26,27] according to the electronegativity equalization principle[57,59] which states that,

at equilibrium, the instantaneous electronegativity χ of each atom has the same value.[57,59] The FQs ($\mathbf{q}$) can be defined as those minimizing the following functional[56]

$$\begin{aligned} F(\mathbf{q},\lambda) =& \sum_{\alpha,i} q_{\alpha i}\chi_{\alpha i} + \frac{1}{2}\sum_{\alpha,i}\sum_{\beta,j} q_{\alpha i}J_{\alpha i,\beta j}q_{\beta j} + \sum_{\alpha}\lambda_{\alpha}(\sum_{i} q_{\alpha i} - Q_{\alpha}) \\ =& \mathbf{q}^{\dagger}\boldsymbol{\chi} + \frac{1}{2}\mathbf{q}^{\dagger}\mathbf{J}\mathbf{q} + \boldsymbol{\lambda}^{\dagger}\mathbf{q} \end{aligned} \tag{1}$$

where $\mathbf{q}$ is a vector containing the FQs, and the Greek indices α run over molecules and the Latin ones i over the atoms of each molecule. $\boldsymbol{\lambda}$ is a set of Lagrangian multipliers used to impose charge conservation constraints on each molecule. The charge interaction kernel $\mathbf{J}$ is, in our implementation, the Ohno kernel.[60] Atomic units are use throughout. The stationarity conditions of the functional in eq.1 are defined through the following equation[56]

$$\mathbf{D}\mathbf{q}_{\boldsymbol{\lambda}} = -\mathbf{C}_{Q} \tag{2}$$

where $\mathbf{C}_Q$ collects atomic electronegativities and total charge constraints, whereas charges and Lagrange multipliers are collected in $\mathbf{q}_{\boldsymbol{\lambda}}$, and $\mathbf{D}$ includes the $\mathbf{J}$ matrix and the Lagrangian blocks.

By following the general philosophy of the so-called "focused" models, in the QM/FQ/PCM model, a classical interaction between the FQs and the QM density is considered:[53]

$$E_{\mathrm{QM/MM}} = \sum_{i=1}^{N_q} V_{\mathrm{QM}}[\rho](\mathbf{r}_i)q_i \tag{3}$$

where $V_{\mathrm{QM}}[\rho](\mathbf{r}_i)$ is the electrostatic potential due to the QM density of charge at the i-th FQ q_i placed at $\mathbf{r}_i$. If a Self Consistent Field (SCF) description of the QM portion is adopted, the global QM/MM energy functional reads:[53,54,61]

$$\mathcal{E}[\mathbf{P},\mathbf{q},\boldsymbol{\lambda}] = \mathrm{tr}\mathbf{h}\mathbf{P} + \frac{1}{2}\mathrm{tr}\mathbf{P}\mathbf{G}(\mathbf{P}) + \mathbf{q}^{\dagger}\boldsymbol{\chi} + \frac{1}{2}\mathbf{q}^{\dagger}\mathbf{J}\mathbf{q} + \boldsymbol{\lambda}^{\dagger}\mathbf{q} + \mathbf{q}^{\dagger}\mathbf{V}(\mathbf{P}) \tag{4}$$

where $\mathbf{h}$ and $\mathbf{G}$ are the one and two electron contributions to the energy and Fock operator, and $\mathbf{P}$ is the density matrix. The FQs consistent with the QM density are obtained by solving the following equation

$$\mathbf{D}\mathbf{q}_{\boldsymbol{\lambda}} = -\mathbf{C}_Q - \mathbf{V}(\mathbf{P}) \tag{5}$$

which includes the coupling term $\mathbf{V}(\mathbf{P})$ between the QM and MM moieties.

By exploiting the definition of $\mathbf{q}$ in Eq. 5, Eq. 4 can be rewritten as follows by neglecting the pure FQ contributions:

$$\begin{aligned} \mathcal{E} &= \operatorname{tr}\mathbf{h}\mathbf{P} + \frac{1}{2}\operatorname{tr}\mathbf{P}\mathbf{G}(\mathbf{P}) + \mathbf{q}^{\dagger}\mathbf{V}(\mathbf{P}) \\ &= \operatorname{tr}\mathbf{h}\mathbf{P} + \frac{1}{2}\operatorname{tr}\mathbf{P}\mathbf{G}(\mathbf{P}) - \mathbf{V}(\mathbf{P})^{\dagger}\mathbf{D}^{-1}\mathbf{V}(\mathbf{P}) \end{aligned} \tag{6}$$

A third layer may be included in the model, by employing a continuum description of the bulk of the solvent,[1] which also allows for an effective and physically suitable way to enforce nonperiodic boundary conditions (nPBC).[56]

Let us consider the expression for PCM energy:[62,63]

$$E_{\mathrm{PCM}} = \operatorname{tr}\mathbf{h}\mathbf{P} + \frac{1}{2}\operatorname{tr}\mathbf{G}(\mathbf{P}) - \frac{f(\varepsilon)}{2}\boldsymbol{\phi}(\mathbf{P})^{\dagger}\mathbf{S}^{-1}\boldsymbol{\phi}(\mathbf{P}) \tag{7}$$

In the explicit PCM term, $\boldsymbol{\phi}$ is the electrostatic potential of the molecule acting on the PCM charges, and the matrix $\mathbf{S}$ is determined by the shape of the cavity (a simple sphere, in our case) and depends upon the apparent surface charge discretization while $f(\varepsilon)$ is a function of the solvent dielectric constant. For simplicity here we assume the use of the conductor-like PCM (CPCM); other PCM models may be used by replacing $\mathbf{S}$ with the proper matrix for the specific flavor of PCM. It is worth to notice the numerical similarity of this expression with Eq. 6. Though the matrices involved in the FQ and PCM equations have drastically different physical meanings, the formal analogies in the resulting mathematical

expressions make it possible to combine the two methods and make it much easier to achieve a numerically efficient combined implementation.

In a three layer QM/MM/PCM model, such as the one that we are considering here, the MM and the PCM portions can be coupled *via* the PCM variational formalism[64] and adding the interaction terms in the energy functional.

$$\begin{aligned}\mathcal{E}[\mathbf{P},\mathbf{q},\boldsymbol{\lambda},\boldsymbol{\sigma}] &= \mathrm{tr}\mathbf{h}\mathbf{P} + \frac{1}{2}\mathrm{tr}\mathbf{P}\mathbf{G}(\mathbf{P}) + \mathbf{q}^{\dagger}\boldsymbol{\chi} + \frac{1}{2}\mathbf{q}^{\dagger}\mathbf{J}\mathbf{q} + \boldsymbol{\lambda}^{\dagger}\mathbf{q} + \mathbf{q}^{\dagger}\mathbf{V}(\mathbf{P}) \\ &+ \frac{1}{2f(\varepsilon)}\boldsymbol{\sigma}^{\dagger}\mathbf{S}\boldsymbol{\sigma} + \boldsymbol{\sigma}^{\dagger}\boldsymbol{\phi}(\mathbf{P}) + \boldsymbol{\sigma}^{\dagger}\boldsymbol{\Omega}\mathbf{q} \end{aligned} \tag{8}$$

where $\mathbf{V}$ and $\boldsymbol{\phi}$ are vectors and denote the QM solute's electrostatic potential calculated at the FQ atoms and at the PCM discretization points, respectively. Notice that electronic quantities such as $\mathbf{P}$, $\mathbf{h}$, and $\mathbf{G}$ are square matrices whose dimension depends on the number of basis functions, but FQ quantities like $\mathbf{q}$ and $\mathbf{J}$ have dimensions that depend on the number of FQ atoms, whereas PCM quantities are also vectors and matrices whose dimension depends on the number of discretization points on the "molecular" surface. Finally, $\mathbf{S}$ and $\boldsymbol{\Omega}$ represent the Coulomb interaction of the PCM charges ($\boldsymbol{\sigma}$) with themselves and with the FQs, respectively. The scaling factor $f(\varepsilon) = \frac{\varepsilon-1}{\varepsilon}$ is used to adjust the results of the conductor-like model (used in this work) to dielectrics. Thus, PCM and FQ charges are solved together with the QM density in the SCF procedure, by exploiting the following linear system:

$$\begin{pmatrix} \mathbf{D} & \boldsymbol{\Omega}^{\dagger} \\ \boldsymbol{\Omega} & \mathbf{S}/f(\varepsilon) \end{pmatrix} \begin{pmatrix} \mathbf{q}_{\boldsymbol{\lambda}} \\ \boldsymbol{\sigma} \end{pmatrix} = - \begin{pmatrix} \mathbf{C} \\ \mathbf{0} \end{pmatrix} - \begin{pmatrix} \mathbf{V}(\mathbf{P}) \\ \boldsymbol{\phi}(\mathbf{P}) \end{pmatrix} \tag{9}$$

2.2 The ROA scattering intensity

The far from resonance (FFR) ROA scattering cross-section for a vibrational transition from a state i to a state j can be written as some combination of three tensors:[65,66]

$$\begin{aligned}
\alpha_{ab} &= \sum_{k\neq j,i}\left(\frac{\langle j|\,\mu_a\,|k\rangle\,\langle k|\,\mu_b\,|i\rangle}{\omega_{ki}-\omega}+\frac{\langle j|\,\mu_b\,|k\rangle\,\langle k|\,\mu_a\,|i\rangle}{\omega_{kj}+\omega}\right)\\
G'_{ab} &= \sum_{k\neq j,i}\left(\frac{\langle j|\,\mu_a\,|k\rangle\,\langle k|\,m_b\,|i\rangle}{\omega_{ki}-\omega}+\frac{\langle j|\,m_b\,|k\rangle\,\langle k|\,\mu_a\,|i\rangle}{\omega_{kj}+\omega}\right)\\
A_{abc} &= \sum_{k\neq j,i}\left(\frac{\langle j|\,\mu_a\,|k\rangle\,\langle k|\,\Theta_{bc}\,|i\rangle}{\omega_{ki}-\omega}+\frac{\langle j|\,\Theta_{bc}\,|k\rangle\,\langle k|\,\mu_a\,|i\rangle}{\omega_{kj}+\omega}\right)
\end{aligned} \tag{10}$$

Where the summations run over all vibronic states, μ, m, and Θ are the electric dipole, magnetic dipole, and electric quadrupole operators, respectively, ω_{ki} denotes the angular frequency difference between states k and i, ω is the laser angular frequency, and the states i and j belong to the same electronic level, while the index j runs over all excited vibrational and electronic states. Since the laser frequency typically falls within the visible range or above, the pure vibrational part of the tensors can be neglected, and only the electronic part is computed.[67] If the ground-state potential energy surface (PES) is treated by means of the harmonic approximation, then these tensors can be rewritten as a combination of normal-mode derivatives of the electronic polarizabilities. By relying on TDDFT as the chosen electronic structure method, the calculation of the spectrum's fundamental bands requires the calculation of geometrical derivatives of the three electronic tensors above. In the following section the theory will be reviewed and the explicit environment contributions to the response functions derivatives will be given.

2.3 Analytical Evaluation of the polarizability derivatives

We now present a detailed description of the implementation for the analytical calculation, based on DFT response theory, of the electronic part of the tensors in equation 10 for an isolated molecule. The presentation of the isolated molecule case precedes the discussion

of solvated systems, treated with the QM/FQ/PCM model, and is necessary to understand which terms in the equations are affected by specific contributions. In the following discussion, an apex is used to denote a derivative, with labels α, β denoting generic field derivatives of field-dependent quantities, x denoting a geometrical derivative, while e, m, and q are used to denote electric field, magnetic field, and electric-quadrupole derivatives, respectively. In terms of the density matrix, the electronic polarizability can be expressed as:

$$\alpha(\omega) = \mathrm{tr}\, \mathbf{h}^{\alpha}\mathbf{P}^{\beta}(\omega) \tag{11}$$

Where $\mathbf{h}$ denotes the one-electron Hamiltonian and $\mathbf{P}$ is the density matrix. For the polarizability proper α, both perturbations are electric, but the indices are kept general because these equations apply for other perturbations as well, provided the basis functions do not depend on the perturbation. Taking its derivative with respect to a geometrical perturbation we get:

$$\alpha^{x}(\omega) = \mathrm{tr}\, \mathbf{h}^{\alpha x}\mathbf{P}^{\beta}(\omega) + \mathrm{tr}\, \mathbf{h}^{\alpha}\mathbf{P}^{\beta x}(\omega) \tag{12}$$

The second derivative of the density matrix appears, which can in principle be obtained through a second-order Coupled-Perturbed Hartree-Fock or Kohn-Sham (CPHF/CPKS) procedure, given here for the occupied (o) and virtual (v) block.

$$(\varepsilon_o - \varepsilon_v + \omega)\mathbf{P}^{\beta x}_{ov}(\omega) - \mathbf{G}(\mathbf{P}^{\beta x}_{ov}(\omega)) = \mathbf{B}^{\beta x}_{ov} \tag{13}$$

where, $\mathbf{B}^{\beta x}$ is[68]

$$\begin{aligned}\mathbf{B}^{\beta x} =& \mathbf{h}^{\beta x} + \mathbf{G}^{x}(\mathbf{P}^{\beta}(\omega)) + \mathbf{G}(\mathbf{P}^{\beta x}_{oo,vv}(\omega)) + \left[\mathbf{F}^{x}, \mathbf{P}^{\beta}(\omega)\right] + \left[\mathbf{F}^{\beta}(\omega), \mathbf{P}^{x}\right] \\ &+ \mathbf{F}^{\beta}(\omega)\mathbf{P}\mathbf{S}^{x} - \mathbf{S}^{x}\mathbf{P}\mathbf{F}^{\beta}(\omega) + \mathbf{F}\mathbf{P}^{\beta}(\omega)\mathbf{S}^{x} - \mathbf{S}^{x}\mathbf{P}^{\beta}(\omega)\mathbf{F} + \omega\{\mathbf{S}^{x}, \mathbf{P}^{\beta}(\omega)\}\end{aligned} \tag{14}$$

$\mathbf{F}$ is the Fock operator, $\mathbf{S}$ is the overlap matrix and $\mathbf{G}$ is the two-electron part of the Fock operator, the braces indicate the anticommutator and

$$\mathbf{P}^{\beta x}_{oo,vv}(\omega) = -\left(\left\{\mathbf{P}^{\beta}(\omega), \mathbf{P}^{x}\right\}_{oo} + \left\{\mathbf{P}^{\beta}(\omega), \mathbf{S}^{x}\right\}_{oo}\right) + \left\{\mathbf{P}^{\beta}(\omega), \mathbf{P}^{x}\right\}_{vv} \tag{15}$$

In this context, the expression in eq. 12 can be separated into contributions from occupied (o) and virtual (v) orbital pairs:

$$\alpha^{x}(\omega) = \operatorname{tr} \mathbf{h}^{\alpha x}\mathbf{P}^{\beta}(\omega) + \operatorname{tr} \mathbf{h}^{\alpha}\mathbf{P}^{\beta x}_{ov,vo}(\omega) + \operatorname{tr} \mathbf{h}^{\alpha}\mathbf{P}^{\beta x}_{oo,vv}(\omega) \tag{16}$$

Since $\mathbf{P}^{\beta x}_{ov}$ is multiplied by a first order term ($\mathbf{h}^{\alpha}$), the equation can be recast by using the interchange relation, that replaces this term with quantities determined by first order CPHF/CPKS.[68–70] Thus, the equation now reads:

$$\alpha^{x}(\omega) = \operatorname{tr} \mathbf{h}^{\alpha x}\mathbf{P}^{\beta}(\omega) + \operatorname{tr} \mathbf{P}^{\alpha}\mathbf{B}^{\beta x}_{ov} + \operatorname{tr} \mathbf{h}^{\alpha}\mathbf{P}^{\beta x}_{oo,vv}(\omega) \tag{17}$$

By further using the following relation:

$$\begin{aligned}\operatorname{tr} \mathbf{h}^{\alpha}\mathbf{P}^{\beta x}_{oo,vv}(\omega) + \operatorname{tr} \mathbf{P}^{\alpha}(\omega)\mathbf{G}(\mathbf{P}^{\beta x}_{oo,vv}(\omega)) &= \operatorname{tr} \mathbf{h}^{\alpha}\mathbf{P}^{\beta x}_{oo,vv}(\omega) + \operatorname{tr} \mathbf{P}^{\beta x}_{oo,vv}(\omega)\mathbf{G}(\mathbf{P}^{\alpha}(\omega)) \\ &= \operatorname{tr} \mathbf{F}^{\alpha}(\omega)\mathbf{P}^{\beta x}_{oo,vv}(\omega)\end{aligned} \tag{18}$$

the expression for the frequency-dependent polarizability derivative becomes:

$$\begin{aligned}\alpha^{x}(\omega) = &\operatorname{tr} \mathbf{h}^{\alpha x}\mathbf{P}^{\beta}(\omega) + \operatorname{tr} \mathbf{P}^{\alpha}(\omega)\mathbf{h}^{\beta x} + \operatorname{tr} \mathbf{P}^{\alpha}(\omega)\mathbf{G}^{x}(\mathbf{P}^{\beta}(\omega)) + \\ &+ \operatorname{tr}\Big\{\mathbf{P}^{\alpha}(\omega)\left(\left[\mathbf{F}^{x}, \mathbf{P}^{\beta}(\omega)\right] + \left[\mathbf{F}^{\beta}(\omega), \mathbf{P}^{x}\right] + \mathbf{F}^{\beta}(\omega)\mathbf{P}\mathbf{S}^{x} - \mathbf{S}^{x}\mathbf{P}\mathbf{F}^{\beta}(\omega) + \right. \\ &\left. + \mathbf{F}\mathbf{P}^{\beta}(\omega)\mathbf{S}^{x} - \mathbf{S}^{x}\mathbf{P}^{\beta}(\omega)\mathbf{F} + \omega\{\mathbf{S}^{x}, \mathbf{P}^{\beta}(\omega)\}\right)\Big\} + \operatorname{tr} \mathbf{F}^{\alpha}(\omega)\mathbf{P}^{\beta x}_{oo,vv}(\omega)\end{aligned} \tag{19}$$

where only density matrix first derivatives are required.

Now we move on to the derivation of the two other tensors for a Fock-like Hamiltonian. For the A tensor the derivation is essentially the same, replacing α with the quadrupole field q and β with the electric field, e.

$$A(\omega) = \mathrm{tr}\, \mathbf{h}^q \mathbf{P}^e(\omega) \tag{20}$$

$$\begin{aligned} A^x(\omega) = & \mathrm{tr}\, \mathbf{h}^{qx} \mathbf{P}^e(\omega) + \mathrm{tr}\, \mathbf{P}^q(\omega) \mathbf{h}^{ex} + \mathrm{tr}\, \mathbf{P}^q(\omega) \mathbf{G}^x(\mathbf{P}^e(\omega)) + \\ & + \mathrm{tr} \Big\{ \mathbf{P}^q(\omega) \left([\mathbf{F}^x, \mathbf{P}^e(\omega)] + [\mathbf{F}^e(\omega), \mathbf{P}^x] + \mathbf{F}^e(\omega) \mathbf{P} \mathbf{S}^x - \mathbf{S}^x \mathbf{P} \mathbf{F}^e(\omega) + \right. \\ & \left. + \mathbf{F} \mathbf{P}^e(\omega) \mathbf{S}^x - \mathbf{S}^x \mathbf{P}^e(\omega) \mathbf{F} + \omega \{ \mathbf{S}^x, \mathbf{P}^e(\omega) \} \right) \Big\} + \mathrm{tr}\, \mathbf{F}^q(\omega) \mathbf{P}^{ex}_{oo,vv}(\omega) \end{aligned} \tag{21}$$

In the case of the G' tensor it is necessary to employ GIAOs to ensure gauge-origin invariance in the results. In the QM framework, these tensors are thus obtained as:[41,71]

$$G'(\omega) = \mathrm{tr}\, \mathbf{F}^{(m)} \mathbf{P}^e(\omega) + \mathrm{tr}\, \mathbf{S}^m \mathbf{W}^e(\omega) + \omega\, \mathrm{tr}\, \bar{\mathbf{S}}^m \mathbf{P}^e(\omega) \tag{22}$$

where m is the magnetic field,

$$\mathbf{F}^{(m)} = \mathbf{h}^m + \mathbf{G}^m(\mathbf{P}) \tag{23}$$

and $\mathbf{W}^e$, the derivative of the energy weighted density matrix:

$$\mathbf{W}^e(\omega) = \mathbf{P}^e(\omega) \mathbf{F} \mathbf{P} + \mathbf{P} \mathbf{F}^e(\omega) \mathbf{P} + \mathbf{P} \mathbf{F} \mathbf{P}^e(\omega) \tag{24}$$

and $\mathbf{S}^m$ and $\bar{\mathbf{S}}^m$ are defined as:

$$\mathbf{S}^m = \langle \psi_\mu | \psi_\nu \rangle^m \tag{25}$$

$$\bar{\mathbf{S}}^m = \langle \psi_\mu | \psi^m_\nu \rangle \tag{26}$$

$$\psi^{m_\gamma}_\mu = -\frac{i}{2c} \left(\mathbf{R}_\mu \times \mathbf{r} \right)_{m_\gamma} \psi_\mu \tag{27}$$

The derivative of a magnetic field-dependent basis functions[42] with respect to the magnetic field appears in the last equation, in which $\mathbf{R}_\mu$ is the position vector of the basis function

ψ_μ, $\mathbf{r}$ is the electronic coordinate and γ is a component of the magnetic field m.

Taking the derivative of eq. 22 with respect to a geometrical perturbation and applying the interchange relation and using

$$\mathbf{F}^{(mx)} = \mathbf{h}^{mx} + \mathbf{G}^{mx}(\mathbf{P}) + \mathbf{G}^{m}(\mathbf{P}^{x}) \tag{28}$$

$$\operatorname{tr} \mathbf{P}^{e}(\omega)\mathbf{G}^{m}(\mathbf{P}^{x}) = \operatorname{tr} \mathbf{P}^{x}\mathbf{G}^{m}(\mathbf{P}^{e}(\omega)) \tag{29}$$

leads to the following expression for G'^{x}:

$$\begin{aligned}
G'^{x}(\omega) = & \operatorname{tr} \mathbf{h}^{mx}\mathbf{P}^{e}(\omega) + \operatorname{tr} \mathbf{P}^{e}(\omega)\mathbf{G}^{mx}(\mathbf{P}) + \operatorname{tr} \mathbf{P}^{x}\mathbf{G}^{m}(\mathbf{P}^{e}(\omega)) + \operatorname{tr} \mathbf{P}^{m}(\omega)\mathbf{h}^{ex} + \operatorname{tr} \mathbf{P}^{m}(\omega)\mathbf{G}^{x}(\mathbf{P}^{e}(\omega)) + \\
& + \operatorname{tr} \Big\{ \mathbf{P}^{m}(\omega) \left([\mathbf{F}^{x}, \mathbf{P}^{e}(\omega)] + [\mathbf{F}^{e}(\omega), \mathbf{P}^{x}] + \mathbf{F}^{e}(\omega)\mathbf{P}\mathbf{S}^{x} - \mathbf{S}^{x}\mathbf{P}\mathbf{F}^{e}(\omega) \right. \\
& \left. + \mathbf{F}\mathbf{P}^{e}(\omega)\mathbf{S}^{x} - \mathbf{S}^{x}\mathbf{P}^{e}(\omega)\mathbf{F} + \omega\{\mathbf{S}^{x}, \mathbf{P}^{e}(\omega)\} \right) \Big\} + \operatorname{tr} \mathbf{F}^{m}(\omega)\mathbf{P}^{ex}_{oo,vv}(\omega) \\
& - \operatorname{tr} \mathbf{W}^{e}(\omega)\mathbf{S}^{mx} - \operatorname{tr} \mathbf{S}^{m} \Big\{ \mathbf{P}^{e}(\omega)\mathbf{F}^{x}\mathbf{P} + \mathbf{P}\mathbf{F}^{x}\mathbf{P}^{e}(\omega) + \mathbf{P}^{x}\mathbf{F}^{e}(\omega)\mathbf{P} + \mathbf{P}\mathbf{F}^{e}(\omega)\mathbf{P}^{x} \\
& + \mathbf{P}^{e}(\omega)\mathbf{F}\mathbf{P}^{x} + \mathbf{P}^{x}\mathbf{F}\mathbf{P}^{e}(\omega) + \mathbf{P}^{ex}_{oo,vv}(\omega)\mathbf{F}\mathbf{P} + \mathbf{P}\mathbf{F}\mathbf{P}^{ex}_{oo,vv}(\omega) \Big\} + \omega \operatorname{tr} \bar{\mathbf{S}}^{m}\mathbf{P}^{ex}_{oo,vv}(\omega) \\
& + \omega \operatorname{tr} \bar{\mathbf{S}}^{mx}\mathbf{P}^{e}(\omega)
\end{aligned} \tag{30}$$

where the additional terms arise from the second and third term in Eq. 22.

The above expressions are general for open and closed shell systems and, remarkably, only require the solution of the first order CPHF/CPKS. These are, however, only applicable to isolated systems, since they lack any explicit terms that would appear when the molecule is embedded in a polarizable environment such as in the QM/FQ/PCM scheme. Note that, similar expressions for the derivatives of $\alpha(\omega)$ and $A(\omega)$ with respect to nuclear coordinates have been presented by Champagne and coworkers for the Hartree-Fock Hamiltonian.[67,72] Expressions for the derivative of $G'(\omega)$ with respect to nuclear coordinates using magnetic field-independent functions[40] and GIAOs[41] haven also been proposed, but only focusing on

molecules in the gas phase.

2.4 QM/FQ/PCM Contributions

As presented in the previous section, response functions for the ROA tensors are derived in the Molecular Orbital (MO) basis. In a QM/FQ/PCM calculation the MO themselves are different because of the presence of the solvent and therefore carry the effect of the environment, providing an indirect solvation effect upon all molecular quantities. There are, however, additional explicit terms that must be added to the equations. These FQ and PCM terms originate from the differentiation of the QM/FQ/PCM energy expression, and they can always be written in terms of derivatives of the potential and charges. One-electron contributions do not pose a problem and can be thought as being included in the terms containing the one-electron Hamiltonian $\mathbf{h}$ in the preceding section. The two-electron contributions, however, give rise to the additional explicit terms. Notice that the following expressions for the FQ contributions are written by explicitly specifying the sum over the atomic basis functions for the sake of clarity. For instance, the FQ contribution to $\left(\mathrm{tr}\,\mathbf{P}^{e}(\omega)\mathbf{G}^{x}\mathbf{P}^{e'}(\omega)\right)$ in eq. 19 is given by:

$$\sum_{\mu\nu}\left[\mathbf{q}^{\dagger}(\mathbf{P}^{e'}(\omega'))\mathbf{V}^{x}_{\mu\nu}P^{e}_{\mu\nu}(\omega)\right]+\sum_{\mu\nu}\left[\mathbf{q}^{\dagger}(\mathbf{P}^{e}(\omega))\mathbf{V}^{x}_{\mu\nu}P^{e'}_{\mu\nu}(\omega')\right] \tag{31}$$

The PCM contribution can be formulated in a similar way. When considering a dynamical field, such as the ones used in Raman and ROA spectroscopy which are usually lasers with wavelength in the visible range, the solvent's response is described by its optical dielectric constant (i.e. the square of the refractive index), rather than the static one, which is used to generate the matrix for the ground-state calculation.

Thus, in terms of PCM charges $\boldsymbol{\sigma}$, the contribution to electric dipole – electric dipole polar-

izability derivatives is:

$$\sum_{\mu\nu}\left[\boldsymbol{\sigma}^{\dagger}(\mathbf{P}^{e'}(\omega'))\boldsymbol{\phi}^{x}_{\mu\nu}P^{e}_{\mu\nu}(\omega)\right]+\sum_{\mu\nu}\left[\boldsymbol{\sigma}^{\dagger}(\mathbf{P}^{e}(\omega))\boldsymbol{\phi}^{x}_{\mu\nu}P^{e'}_{\mu\nu}(\omega')\right] \tag{32}$$

In standard PCM calculations, there is also another contribution due to the derivative of the PCM matrix with respect to x, because as the solute atoms move so does the cavity, which is usually defined in terms of spheres centered on the atoms. In the case considered here these terms do not appear because in the QM/FQ/PCM the PCM layer originates from a fixed spherical cavity which does not move with the solute atoms. Next we will follow the same derivation to evaluate QM/FQ/PCM contributions to the other tensors. By comparing eq. 21 and eq.19, it is evident that the two expressions are analogous. Therefore, the QM/FQ contributions to $\left(\mathrm{tr}\,\mathbf{P}^{\alpha}(\omega)\mathbf{G}^{x}\mathbf{P}^{\beta}(\omega)\right)$ for A^{x} can be expressed in the following way:

$$A^{x}(\omega)_{QM/FQ}=\sum_{\mu\nu}\left[\mathbf{q}^{\dagger}(\mathbf{P}^{e}(\omega))\mathbf{V}^{x}_{\mu\nu}P^{q}_{\mu\nu}\right]+\sum_{\mu\nu}\left[\mathbf{q}^{\dagger}(\mathbf{P}^{q})\mathbf{V}^{x}_{\mu\nu}P^{e}_{\mu\nu}(\omega)\right] \tag{33}$$

The above formula is obtained by substituting e with q in Eq. 31. If an outer PCM layer is present (a fixed spherical cavity is considered, as explained above) an additional contribution appears. In particular, eq. 32 is to be modified in order to depend on the quadrupole field, so that it reads:

$$A^{x}(\omega)_{QM/PCM}=\sum_{\mu\nu}\left[\boldsymbol{\sigma}^{\dagger}(\mathbf{P}^{e}(\omega))\boldsymbol{\phi}^{x}_{\mu\nu}P^{q}_{\mu\nu}\right]+\sum_{\mu\nu}\left[\boldsymbol{\sigma}^{\dagger}(\mathbf{P}^{q})\boldsymbol{\phi}^{x}_{\mu\nu}P^{e}_{\mu\nu}(\omega)\right] \tag{34}$$

Let us move on to G'^{x}. By looking at eq. 30, we see that similar contributions to the ones already introduced for the two other tensors have to be considered. In particular, the contribution of the FQs to $\mathrm{tr}\,\mathbf{P}^{e}(\omega)\mathbf{G}^{x}\Big(\mathbf{P}^{m}(\omega)\Big)$ becomes:

$$\sum_{\mu\nu}\left[\mathbf{q}^{\dagger}(\mathbf{P}^{m})\mathbf{V}^{x}_{\mu\nu}P^{e}_{\mu\nu}(\omega)\right]+\sum_{\mu\nu}\left[\mathbf{q}^{\dagger}(\mathbf{P}^{e}(\omega))\mathbf{V}^{x}_{\mu\nu}P^{m}_{\mu\nu}\right] \tag{35}$$

The previous equation is obtained by substituting e' with m in Eq. 31. If an outer PCM layer is present, eq. 32 must be modified in order to depend on the magnetic field:

$$\sum_{\mu\nu}\left[\boldsymbol{\sigma}^{\dagger}(\mathbf{P}^{m})\boldsymbol{\phi}^{x}_{\mu\nu}P^{e}_{\mu\nu}(\omega)\right]+\sum_{\mu\nu}\left[\boldsymbol{\sigma}^{\dagger}(\mathbf{P}^{e}(\omega))\boldsymbol{\phi}^{x}_{\mu\nu}P^{m}_{\mu\nu}\right] \tag{36}$$

Two additional terms appear due to the presence of the magnetic field within the GIAO formalism. By resorting once again to the similarity between the FQ and PCM formalisms, the first contribution to the $\mathrm{tr}\,\mathbf{P}^{x}\mathbf{G}^{m}(\mathbf{P}^{e}(\omega))$ term reads:

$$\mathrm{tr}\,\mathbf{P}^{x}\mathbf{G}^{m}(\mathbf{P}^{e}(\omega))_{QM/FQ}=\sum_{\mu\nu}\left[\mathbf{q}^{\dagger}(\mathbf{V}^{m}(\mathbf{P}^{e}(\omega)))P^{x}_{\mu\nu}\mathbf{V}_{\mu\nu}\right] \tag{37}$$

and, if an outer PCM layer is present, another term has to be included, which reads

$$\mathrm{tr}\,\mathbf{P}^{x}\mathbf{G}^{m}(\mathbf{P}^{e}(\omega))_{QM/PCM}=\sum_{\mu\nu}\left[\boldsymbol{\sigma}^{\dagger}(\boldsymbol{\phi}^{m}(\mathbf{P}^{e}(\omega)))P^{x}_{\mu\nu}\boldsymbol{\phi}_{\mu\nu}\right] \tag{38}$$

In addition to the terms in eqs.37 and 38, a further contribution has to be computed for the $\mathrm{tr}\,\mathbf{P}^{e}(\omega)G^{mx}(\mathbf{P})$ term, having the following expression:

$$\mathrm{tr}\,\mathbf{P}^{e}(\omega)G^{mx}(\mathbf{P})_{QM/FQ}=\sum_{\mu\nu}\left[\mathbf{q}^{\dagger}\mathbf{V}^{m,x}_{\mu\nu}P^{e}_{\mu\nu}(\omega)+\mathbf{q}^{x\dagger}\mathbf{V}^{m}_{\mu\nu}P^{e}_{\mu\nu}(\omega)\right] \tag{39}$$

with the corresponding PCM contribution as:

$$\mathrm{tr}\,\mathbf{P}^{e}(\omega)G^{mx}(\mathbf{P})_{QM/PCM}=\sum_{\mu\nu}\left[\boldsymbol{\sigma}^{\dagger}\boldsymbol{\phi}^{m,x}_{\mu\nu}P^{e}_{\mu\nu}(\omega)+\boldsymbol{\sigma}^{x\dagger}\boldsymbol{\phi}^{m}_{\mu\nu}P^{e}_{\mu\nu}(\omega)\right] \tag{40}$$

We refer the reader to the Appendix for further details on the equations and implementation. After evaluating all the tensor derivatives, the spectroscopic intensities can then be easily assembled once the electronic Hessian has been diagonalized to generate the normal modes of vibration.

We note that in the derivation above only the solute vibrations are considered, thus no geometrical derivatives of the energy with respect to the position of the MM atoms are evaluated. This choice is consistent with the so-called Partial Hessian Vibrational Approach[73] (PHVA), which was already exploited by some of us for the formulation of analytical second derivatives with respect to nuclear coordinates.[74] Also, it is worth spending a few words on the similarities between the QM/FQ Hamiltonian and the QM/PCM one. The QM/FQ model, as it has been thought by the authors of the first implementation, has the same mathematical foundations as the PCM: both models are purely electrostatic and both are characterized by point charges that interact classically with the QM portion. Therefore, the close similarity between the final expressions of polarizability derivatives must not surprise the reader.

3 Computational details

A QM/FQ/PCM calculation involves a number of steps, which are here outlined:

1. *Definition of the system:* the solute is embedded within a sufficiently large number of solvent molecules, chosen so that both the dynamics and the subsequent QM calculations can capture all the relevant solute-solvent interactions.

2. *Classical MD simulation and sampling:* In order to sample the phase space of the system, classical MD simulations are performed. Such simulations are run long enough to sample a sufficiently large portion of the phase-space and such that the simulation parameters correctly reproduce all possible system configurations and their relative energy (and thus population). From the MD simulations a number of snapshots are extracted to be used later in the QM/FQ/PCM calculations.

3. *Definition of the different regions of the three-layer scheme and their boundaries:* for each snapshot extracted from the dynamics, a sphere centered on the solute is cut,

retaining all solvent molecules within the sphere and discarding the rest. The radius of this region is chosen to simulate all specific solute-solvent interactions, while bulk solvent properties are modeled by covering the sphere in a polarizable continuum whose interaction with the solute is modeled by the PCM.

4. *Running the QM/FQ/PCM calculations on the snapshots:* once all the snapshots have been obtained, and the system has been partitioned into the different layers and their boundaries defined, the calculation of Raman/ROA is performed. The geometry of the solute in each snapshot is optimized, holding fixed the position and the geometries of all the solvent molecules.

5. *Analysis of the result:* the results obtained for each snapshot are extracted and pooled to produce the final spectrum.

More computational details about each of these steps that have been used in the calculations presented in this work are as follows. Molecular geometries were optimized at the B3LYP/aug-cc-pVDZ level, including solvent effects using C-PCM[62,63] and default cavity parameters used to represent the aqueous environment. The molecular dynamics simulations were carried out as detailed in previous works[9] using GROMACS.[75] A total of 2000 snapshots were extracted from the last 20 ns of the MD simulation (one snapshot every 10 ps), but only 200 snapshots were used to generate the spectra following an analysis on the convergence behavior of the spectra with respect to snapshot number (vide infra). For each snapshot a sphere centered at the solute's geometric center was cut. A cutting radius of 12 Å was used, surrounded by a 1.5 Å larger radius for the PCM spherical cavity. The partial geometry optimization of each snapshot was performed keeping the water molecules fixed. Finally, all spectra were calculated within a QM/FQ/PCM framework using the B3LYP functional with the aug-cc-pVDZ basis set for the solute, the SPC FQ parameters[26] and the C-PCM to account for the aqueous environment. Non-polarizable QM/MM calculations were performed using the TIP3P parametrization for water.[76] ROA

measurements may be realized through a multitude of experimental configurations, related to the angle between the incident and scattered radiations, as well as their respective polarizations.[66] In the following, for (R)-methyloxirane, Raman spectra refer to 90° scattering, while ROA spectra are in the back-scattered scattered-circularly-polarized radiation configuration. For (S)-methyllactate, Raman spectra refer to 180° scattering, while ROA spectra are in the back-scattered scattered-circularly-polarized radiation configuration. To convolute the peaks, Lorentzian functions were used, with full width at half maximum (FWHM) of $4\,\mathrm{cm}^{-1}$.[77] All the QM calculations were performed by using a development version of Gaussian package.[78]

4 Results

4.1 Raman and ROA of (R)-methyloxirane

We consider first (R)-methyloxirane (moxy), a very small chiral system whose spectroscopic properties have been studied extensively in the past. We used this system to validate our implementation by comparing results of a frequency-dependent ROA calculation evaluated using both a fully analytical method, and by computing numerical derivatives of the frequency-dependent mixed polarizability tensors. Table 1 reports the results of both calculations. Results are reported in units of $\mathrm{AA}^4/\mathrm{amu}$ and they need to be multiplied by K before being plotted, where K is in cgs units:

$$K = \frac{1}{90}\left(\frac{\omega_\mathrm{s}}{c}\right)^4 \frac{E^2}{R^2} \tag{41}$$

In the expression above, ω_s is the angular frequency of the scattered radiation, R is the distance from the sample to the detector, and E is the magnitude of the incident electric field at the molecular origin.[77] As can be seen from the table, the difference between the results from the two derivative methods are minimal, with the highest difference being 0.0030. Though

the numerical results appear very stable, being able to perform the calculation analytically is particularly advantageous for QM/FQ/PCM calculations because the reduction in the computational cost applies to all snapshots, and can add up to a very significant computational saving, particularly for large systems or for a large number of snapshots. We also performed the same analysis on Raman intensities, which presented even smaller difference between numerical and analytical results (see Supporting Information).

Table 1. Comparison between analytical and numerical ROA intensities (units of K, see Eq. 41) computed for an incident wavelength of 532 nm.

Modes	Analytical	Numerical	Differences
218.7130	4.8940	4.8940	0.0000
377.2240	15.2020	15.2020	0.0000
422.0177	4.3240	4.3240	0.0000
756.3885	-124.0190	-124.0190	0.0000
841.6365	137.5610	137.5600	0.0010
905.5113	118.7660	118.7660	0.0000
965.0963	-19.0860	-19.0860	0.0000
1041.3528	-95.7300	-95.7300	0.0000
1122.1619	39.4840	39.4840	0.0000
1153.3137	-54.6160	-54.6160	0.0000
1174.0052	39.9070	39.9070	0.0000
1184.4206	59.2400	59.2400	0.0000
1290.2361	-46.4500	-46.4500	0.0000
1384.5402	-13.8670	-13.8670	0.0000
1430.0974	95.7010	95.7010	0.0000
1460.7858	76.3990	76.3990	0.0000
1474.8403	-231.3600	-231.3600	0.0000
1520.4632	55.5550	55.5550	0.0000
3044.7759	144.5140	144.5140	0.0000
3116.0928	-877.8090	-877.8100	0.0010
3118.3139	1066.2760	1066.2750	0.0010
3141.7886	-28.4640	-28.4670	0.0030
3174.3436	341.5490	341.5490	0.0000
3217.8385	-642.9800	-642.9810	0.0010

It has been shown in previous studies that in order to accurately simulate a chiral property such as optical rotation (OR) of this system, a very large number of snapshots (≥ 2000) was necessary to achieve convergence.[9] However, Raman and ROA intensities are not expected to require the same large number of snapshots to achieve convergence, as they are related to

intrinsically local molecular properties, while OR is a global electronic property of the system. This fact is particularly relevant because ROA intensities are related to the geometrical derivatives of the very same tensors that generate optical activity, thus the process of taking the derivative with respect to atomic positions localizes the effect induced by the solvent. In practice, our tests indicate that for moxy 200 snapshots are enough to achieve convergence in ROA calculations (data shown in the Supporting Information), 10% of those required for OR. It is thus evident from the results that the derivatives of the Raman and ROA tensors with respect to the normal modes are rather flat. The low number of snapshots required may also be due to the structural rigidity of methyloxirane, whose vibrational modes are not significantly altered by the presence of the solvent. A more flexible solute, however, might experience significant changes in its vibrational modes when in the presence of the solvent, therefore our considerations on methyloxirane cannot be a priori extended to the general case and convergence with respect to the number of snapshots should in general be considered on a case-by-case basis. The question of convergence in the spectra is closely related to the dispersion of the computed property across the phase space sampled during the MD simulation. In figures 2.1 and 2.2 the unconvoluted results are presented as stick spectra for the first 200 snapshots of the simulation. The dispersion of the peaks is not particularly high, and for the ROA intensities there are only few cases where different snapshots would give bands of opposite sign with respect to the average.

Finally, we can compare the computed results with available Raman[79] and ROA[80] experimental data (figures 3.1 and 3.2, respectively). Both the experimental spectra refer to neat liquid moxy, not the aqueous solution, therefore some differences with the computed results are expected. To the best of our knowledge there are no available spectra for the molecule in water. In figure 3.1 the QM/FQ/PCM Raman spectrum is compared to experiment[79] and to a spectrum computed using a non-polarizable QM/MM method where the solvent charges are fixed. The QM/FQ/PCM and the QM/MM results are very close, particularly in terms of intensities. The most evident differences are in the position of the bands, hence the

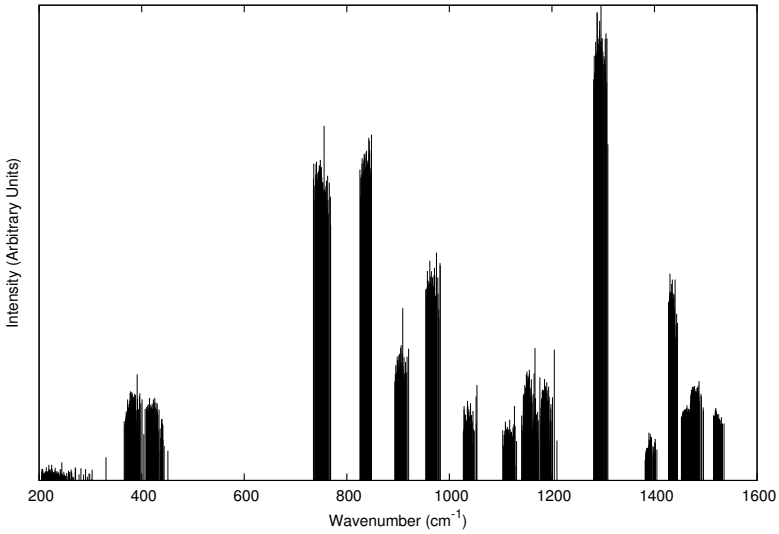

(2.1). Raman

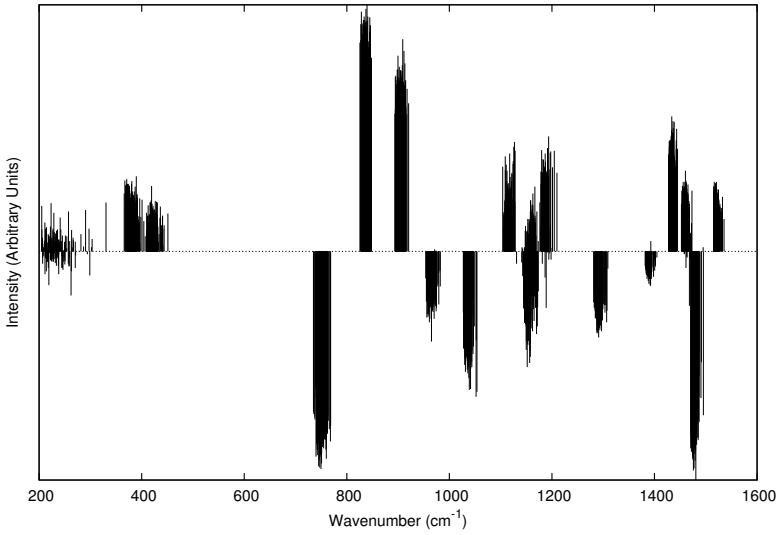

(2.2). ROA

Figure 2. Unconvoluted QM/FQ/PCM Raman and ROA spectra of moxy, where the intensity from each of the 200 snapshots is plotted individually.

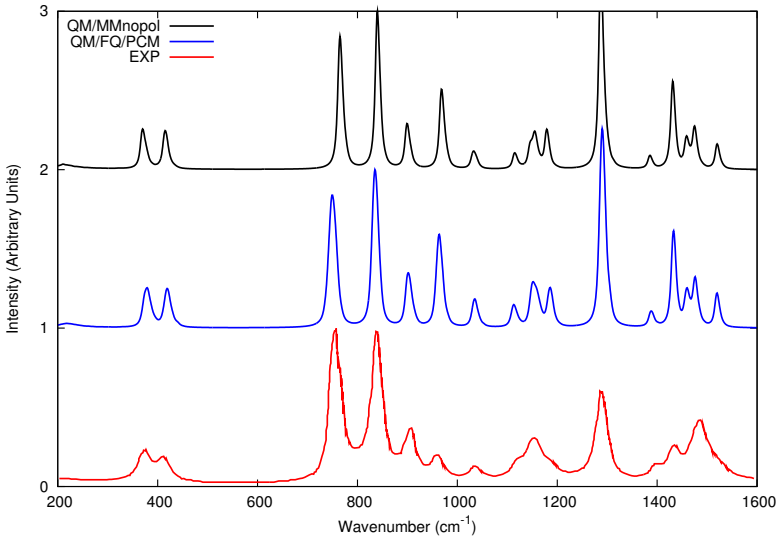

(3.1). Raman

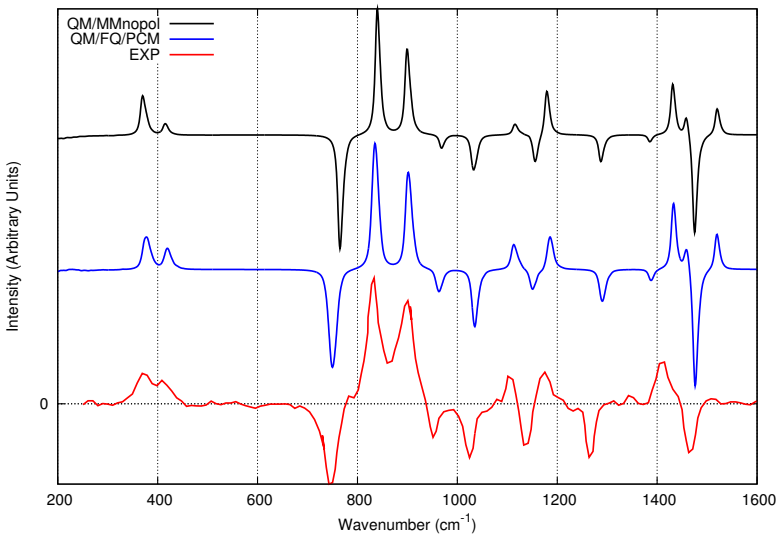

(3.2). ROA

Figure 3. Convoluted QM/FQ/PCM Raman and ROA spectra of moxy, where each of the peaks from figure 2 is convoluted with a Lorentzian function of full-width-at-half-maximum of $4\,\mathrm{cm}^{-1}$.

vibrational frequencies, which are slightly red-shifted in the case of a polarizable force-field. This brings the computed spectrum in closer agreement to experiment, although it should be mentioned that our results rely on the harmonic approximation, and anharmonicity effects would be expected to further red-shift the results. Both methods reproduce experimental findings quite accurately despite the fact that, as already mentioned above, the experimental spectrum was measured on the neat liquid. Our calculation would suggest that the presence of water would not significantly alter the vibrational properties of this molecule. Similar conclusions can be reached for the ROA spectra, shown in figure 3.2. In this case the effect of polarization does not change the spectrum in a significant way and both methods are able to reproduce the experimental spectrum. One noticeable difference is the high intensity of the negative band at $1475\,\mathrm{cm}^{-1}$ which is quenched in the experimental spectrum. A possible explanation is an error in the calculation of the frequency for the positive band around $1520\,\mathrm{cm}^{-1}$, which is also quenched in the experimental spectrum. If these two bands were to overlap more, then the positive and negative contributions would cancel out. A larger band width would achieve a similar effect. Note that in the Raman spectrum, the positive band appears as an isolated peak in the computed spectrum whereas there is only one wide band in the experimental spectrum.

4.2 (S)-Methyl-lactate

In this section we investigate the Raman and ROA spectra of (S)-methyl-lactate (MLac), which exists in three distinct conformations, depicted in figure 4 along with their QM/PCM Boltzmann populations, which include harmonic thermal vibrational contributions. The first conformer is by far the most stable and therefore abundant thanks to the intra-molecular hydrogen bond, with the other two conformers adding up only to a 21% population. The conformational space sampled by the classical simulation can be dramatically different thanks to the effect of the solvent. In particular, the intramolecular hydrogen bond may not be energetically favored compared to the intermolecular one that can form between MLac and

water. We therefore analyzed the conformational distribution from the classical dynamics in terms of two dihedral angles, defined in figure 5. The plot in figure 6 reports the distribution of the dihedral values for the 200 snapshots as well as the three QM/PCM conformations. It can be seen that most of the classical points accumulate around a structure that is not present among the three QM/PCM ones, that is similar to the first and most stable conformer in terms of the first dihedral angle, but where the OH group is oriented toward the solvent. The OH group is in fact very mobile, as can be observed from the figure, and it does not seem to form an intramolecular hydrogen bond as in the first QM/PCM conformation (the red point at the center of the plot in figure 6). The second QM/PCM conformation is the leftmost red dot in the plot, and there are only a few points close to it, whereas the third, and least populated, conformation is not sampled at all by the classical dynamics. These conformational changes can be expected to strongly affect the spectrum.

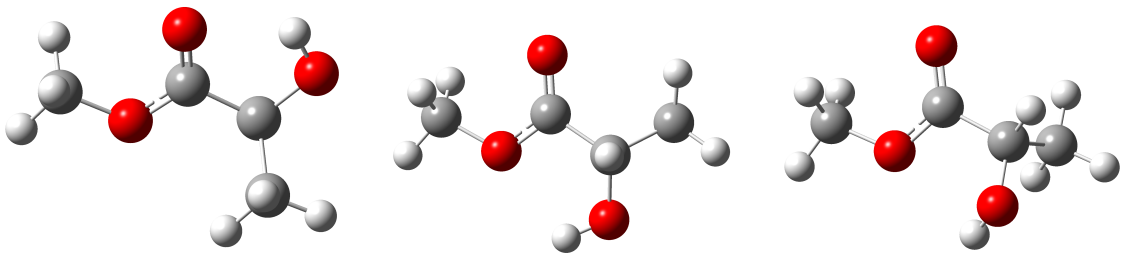

(4.1). 79% **(4.2).** 14% **(4.3).** 7%

Figure 4. MLac conformers. QM/PCM Boltzmann populations are also reported.

Figure 7 reports the experimental[81] as well as the calculated Raman spectrum with the QM/FQ/PCM method. Unfortunately we were unable to find experimental Raman and ROA spectra performed on aqueous solutions, therefore we resort to comparing computed results with experiments carried on neat liquids, as in the case of methyloxirane. Compared to experiment, the predicted QM/FQ/PCM spectrum is very similar, with most features of the spectrum correctly reproduced. The experimental intensities are, for some peaks in the

Figure 5. Definition of the two dihedral angles used in the conformational analysis. The first (Dihderal 1) angle is defined by atoms O1-C2-C3-O4, the second (Dihedral 2) by atoms C2-C3-O4-H5.

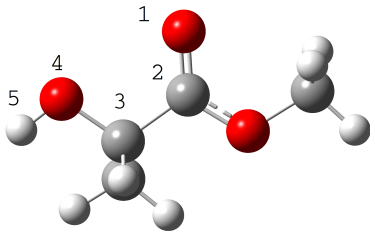

Figure 6. Conformational distribution of MLac from the classical dynamics. Blue crosses represent snapshots, red circles represent the three QM/PCM structures. The two dihedral angles are defined in figure 5.

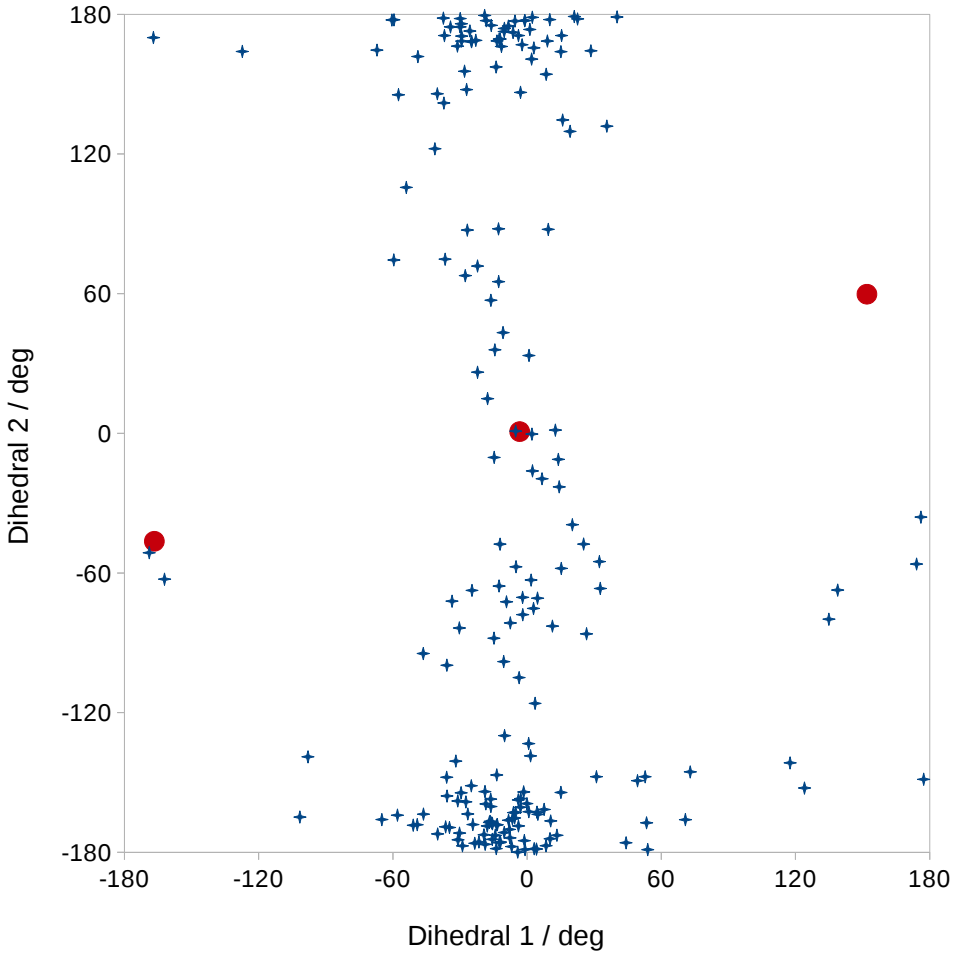

lower-energy region of the spectrum, very high. This is the case for instance, for the mode at 850 cm^{-1}, which corresponds to a highly diffuse concerted bending of the whole molecule, the mode at 980 cm^{-1}, which is mainly a CH_3-O stretching, and the one at 1100 cm^{-1}which is another bending motion. Our model is again able to reproduce such features of the experimental spectrum, except for the mode at 980 cm^{-1}which is much lower in our computations.

Figure 7. Raman spectrum of MLac, 488nm radiation. (top, blue) Calculated QM/FQ/PCM spectrum. (bottom, red) Experimental[81] spectrum.

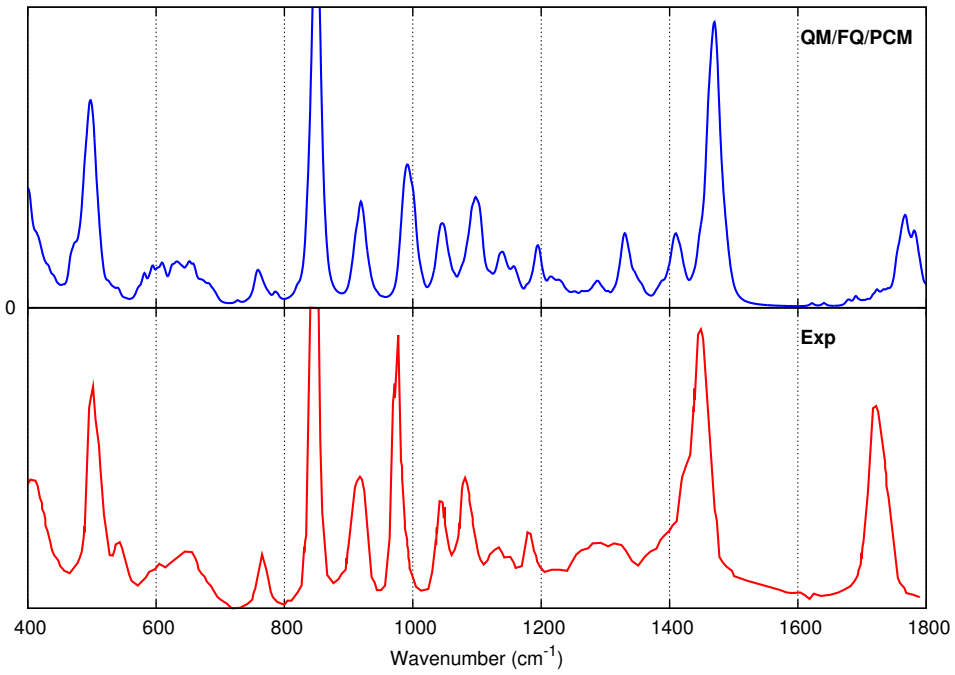

Figure 8 reports a comparison of the calculated QM/PCM and QM/FQ/PCM and experimental[82] ROA spectra. These data refer to a 532 nm incident wavelength and backscattered circularly polarized radiation. The QM/FQ/PCM performs much better than QM/PCM in the comparison. Overall, the QM/PCM and QM/FQ/PCM produce similar spectra in terms of the sign of the band (with few exceptions discussed below), and band positions are also very similar. The QM/FQ/PCM results, however, appear more dispersed for some bands, for example in the case of the negative band at 650 cm^{-1} where the QM/FQ/PCM method produces a much wider negative band compared to the sharp negative peak predicted by the

Figure 8. ROA spectra of MLac, 532 nm incident wavelength and backscattered circularly polarized radiation. (Continuous blue) Calculated QM/FQ/PCM spectrum. (Continuous black) QM/PCM spectrum. (Dashed red) Experimental[82] spectrum.

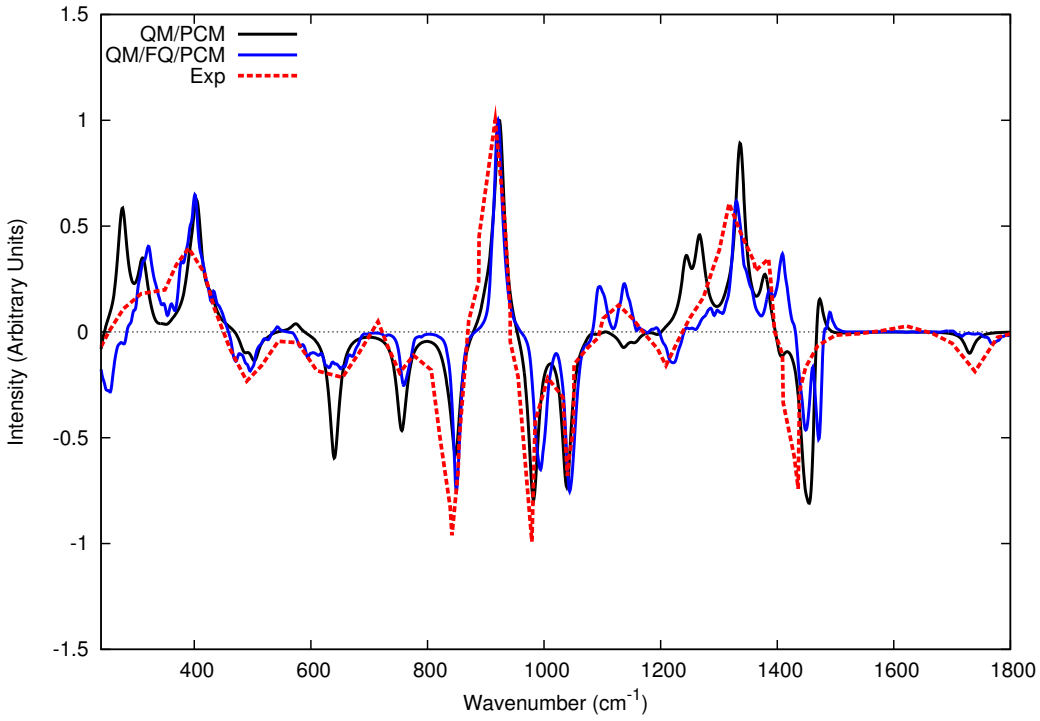

Figure 9. Difference between the ROA intensity for the CO stretching mode of MLac, computed with and without fluctuating polarization effects, for each snapshot. The horizontal red line represents the average QM/FQ/PCM intensity.

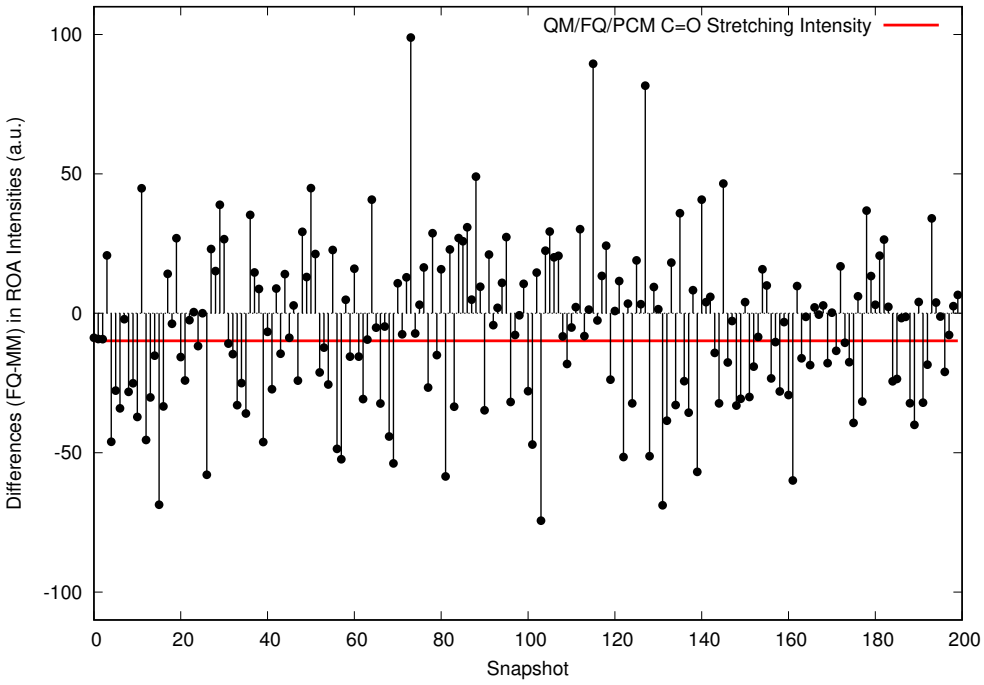

QM/PCM calculation. Note that this is not simply a consequence of a different bandwidth chosen for the convolution for either spectrum because other bands, such as the strongly positive band at 900 cm^{-1} and the weakly positive band 400 cm^{-1}, are instead almost identical for the two methods. The differences discussed for the aforementioned band and for others, are due to the ability of the FQ/PCM method to better sample the system's phase space and more accurately reproduce the solute-solvent interaction. The most evident differences appear in the region between 1000 and 1600 cm^{-1}. At 1140 cm^{-1} both the QM/FQ/PCM method and the experimental data present a weakly positive signal, whereas QM/PCM predicts a weakly negative band, corresponding to the C-OH stretching vibration. Other improvements brought by the QM/FQ/PCM method can be observed in the two strongest bands of the QM/PCM spectrum, a positive signal at 1300 cm^{-1} and a negative signal at 1450 cm^{-1}. The relative intensities of these bands are not as strong in the experimental spectrum, and the QM/FQ/PCM method brings significant improvements in the modeling

of these bands. One major difference between the QM/PCM and QM/FQ/PCM models is that the latter is based on a classical dynamics to sample the configuration space of the system, however once the snapshots have been obtained the subsequent QM calculation could in principle employ a non-polarizable force field for the solvent. The consequences of neglecting polarization effects can be noticed in figure 9, where for each snapshot we report the difference between the ROA intensities of the CO stretching band computed with and without FQ polarization. Notice that to compute ROA intensities without polarization the geometry of the target molecule in each snapshot has been reoptimized because polarization effects also modify the molecular force field. The choice of the CO stretching mode was made because its energy is well separated from all the other modes, therefore it is easy to identify in the results without inspecting the normal modes of each snapshot separately by hand, given the fact that the vibrational energies themselves change. The red line in the graph represents the averaged QM/FQ/PCM value. It can be seen that the difference between the two models is huge in relative terms, and does not seem to have a recognizable trend as the sign can be either positive or negative depending on the specific snapshot.

5 Conclusions and Perspectives

We have presented the first formulation and analytical implementation of FFR Raman and ROA spectra of molecular systems in solution using the fully polarizable multi-layer quantum-classical QM/FQ/PCM model, where the QM portion is modeled *via* TDDFT, and the MM region is described by using the FQ model, with an additional outer PCM layer used to account for bulk solvent effects. The interaction between the solute and both the discrete and the continuum solvent results in additional terms in the QM Hamiltonian that depend on the QM density, and must therefore be determined self-consistently. Solute-solvent interaction terms also appear at all orders of the system's response functions, resulting in additional terms in the evaluation of the response functions and derivatives. In the case

of ROA, additional terms must be considered to ensure gauge-origin independence of the results.

The application of the model to selected systems in aqueous solution shows that in cases where there is a direct solute-solvent interaction that cannot be modeled solely using a continuum model, the QM/FQ/PCM results can be significantly different from those obtained using a standard QM/PCM method, and the agreement with experimental data also improves. The method's reliance on a molecular dynamics to sample the phase space of the system means the computed results are obtained as an average over a large number of snapshots. Assuming the dynamics has adequately sampled all relevant solute geometries, our results show that convergence is achieved rapidly, i.e. Raman and ROA spectra are not significantly affected by the solvent's distribution around the solute, though the FQ model may still be necessary to treat specific effects such as those arising from hydrogen bonds established between solute and solvent. This is in contrast to previous studies on different properties such as Optical Rotation, which is closely related to ROA through the mixed electric-magnetic polarizability tensor. Though ROA is a higher-order property, because of the local nature of molecular vibrations the effect of the solvent is not as drastic. The method presented in this contribution represents a step forward in the modeling of spectroscopic properties of solvated systems, although in order to expand its applicability, accurate parametrizations for other types of solvents is required. In addition, while polar solvents may usually be modeled using electrostatic interactions only, apolar environments such as those generated by solvents like tetrachloromethane or benzene may require an accurate modeling of non-electrostatic repulsion and dispersion effects as well in order to provide reliable results. Such developments could greatly expand the applicability of the present method, towards both more diverse solvents as well as more complex environments, and will be the subject of future research.

6 Acknowledgements

The authors thank Gianluca Del Frate (SNS, Pisa) for his help with MD simulations of MLac. The computer resources provided by the high performance computer facilities of the SMART Laboratory (http://smart.sns.it/) are acknowledged. F.E. acknowledges funding from the European Research Council under the European Union's Seventh Framework Programme (FP/2007-2013)/ERC Grant Agreement n. [320951].

7 Appendix

In this Appendix we expand on the matrial presented in Section 2.4 in order to evaluate Raman/ROA tensors in the QM/FQ/PCM approach.

- QM/FQ/PCM contributions to $\mathrm{tr}\,\mathbf{P}^{\alpha}(\omega)\mathbf{G}^{x}\mathbf{P}^{\beta}(\omega)$, whose expressions are

  for $\alpha^{x}(\omega)$:

$$\sum_{\mu\nu}\left[\mathbf{q}^{\dagger}(\mathbf{P}^{e'}(\omega'))\mathbf{V}^{x}_{\mu\nu}P^{e}_{\mu\nu}(\omega)\right]+\sum_{\mu\nu}\left[\mathbf{q}^{\dagger}(\mathbf{P}^{e}(\omega))\mathbf{V}^{x}_{\mu\nu}P^{e'}_{\mu\nu}(\omega')\right]+$$
$$+\sum_{\mu\nu}\left[\boldsymbol{\sigma}^{\dagger}(\mathbf{P}^{e'}(\omega'))\boldsymbol{\phi}^{x}_{\mu\nu}P^{e}_{\mu\nu}(\omega)\right]+\sum_{\mu\nu}\left[\boldsymbol{\sigma}^{\dagger}(\mathbf{P}^{e}(\omega))\boldsymbol{\phi}^{x}_{\mu\nu}P^{e'}_{\mu\nu}(\omega')\right]$$

  for $A^{x}(\omega)$:

$$\sum_{\mu\nu}\left[\mathbf{q}^{\dagger}(\mathbf{P}^{e}(\omega))\mathbf{V}^{x}_{\mu\nu}P^{q}_{\mu\nu}\right]+\sum_{\mu\nu}\left[\mathbf{q}^{\dagger}(\mathbf{P}^{q})\mathbf{V}^{x}_{\mu\nu}P^{e}_{\mu\nu}(\omega)\right]+$$
$$+\sum_{\mu\nu}\left[\boldsymbol{\sigma}^{\dagger}(\mathbf{P}^{e}(\omega))\boldsymbol{\phi}^{x}_{\mu\nu}P^{q}_{\mu\nu}\right]+\sum_{\mu\nu}\left[\boldsymbol{\sigma}^{\dagger}(\mathbf{P}^{q})\boldsymbol{\phi}^{x}_{\mu\nu}P^{e}_{\mu\nu}(\omega)\right]$$

for $G'^{x}(\omega)$:

$$\sum_{\mu\nu}\left[\mathbf{q}^{\dagger}(\mathbf{P}^{m})\mathbf{V}^{x}_{\mu\nu}P^{e}_{\mu\nu}(\omega)\right]+\sum_{\mu\nu}\left[\mathbf{q}^{\dagger}(\mathbf{P}^{e}(\omega))\mathbf{V}^{x}_{\mu\nu}P^{m}_{\mu\nu}\right]$$
$$+\sum_{\mu\nu}\left[\boldsymbol{\sigma}^{\dagger}(\mathbf{P}^{m})\boldsymbol{\phi}^{x}_{\mu\nu}P^{e}_{\mu\nu}(\omega)\right]+\sum_{\mu\nu}\left[\boldsymbol{\sigma}^{\dagger}(\mathbf{P}^{e}(\omega))\boldsymbol{\phi}^{x}_{\mu\nu}P^{m}_{\mu\nu}\right]$$

The similarities in the expressions above can be exploited in the implementatio of the code required to evalute each term. In particular, the main steps involved are as follows:

1. Compute the density matrix derivative with respect to the external fields (electric, magnetic, or electric quadrupole).
2. Use these derivatives to construct the electronic potential $\mathbf{V}(\mathbf{P}^{i})$, where i indicates the electric, magnetic or quadrupole fields.
3. Evaluate the new set of FQ and PCM charges, by solving Eq. 9.
4. Contract the potential derivatives $\mathbf{V}^{x}(\mathbf{P}^{i})$ with the new set of charges.
5. Sum up the QM/FQ contribution and the QM/PCM one.

- QM/FQ/PCM contributions to $\mathrm{tr}\,\mathbf{P}^{x}\mathbf{G}^{m}(\mathbf{P}^{e}(\omega))$, only applying to G'^{x}:

$$\sum_{\mu\nu}\left[\mathbf{q}^{\dagger}(\mathbf{V}^{m}(\mathbf{P}^{e}(\omega)))P^{x}_{\mu\nu}\mathbf{V}_{\mu\nu}\right]+\sum_{\mu\nu}\left[\boldsymbol{\sigma}^{\dagger}(\boldsymbol{\phi}^{m}(\mathbf{P}^{e}(\omega)))P^{x}_{\mu\nu}\boldsymbol{\phi}_{\mu\nu}\right]$$

The evaluation of this term requires the following steps:

1. Compute the density matrix derivative with respect to the external electric field.
2. Construct the electronic potential $\mathbf{V}(\mathbf{P}^{e})$ and then its derivative with respect to the magnetic field.
3. Evaluate the new set of FQ and PCM charges by solving Eq. 9.
4. Contract the new set of charges with $\mathbf{P}^{x}\mathbf{V}$.

5. Sum up the QM/FQ and QM/PCM contributions.

- QM/FQ/PCM contributions to $\mathrm{tr}\,\mathbf{P}^e(\omega)G^{mx}(\mathbf{P})$, only applying to G'^x:

$$\sum_{\mu\nu}\left[\mathbf{q}^\dagger\mathbf{V}^{m,x}_{\mu\nu}P^e_{\mu\nu}(\omega)+\mathbf{q}^\dagger(\mathbf{V}^m\mathbf{P}^e(\omega))\mathbf{V}^x_{\mu\nu}\mathbf{P}_{\mu\nu}\right]+$$
$$\sum_{\mu\nu}\left[\boldsymbol{\sigma}^\dagger\boldsymbol{\phi}^{m,x}_{\mu\nu}P^e_{\mu\nu}(\omega)+\boldsymbol{\sigma}^\dagger(\boldsymbol{\phi}^m\mathbf{P}^e(\omega))\boldsymbol{\phi}^x_{\mu\nu}\mathbf{P}_{\mu\nu}\right]$$

The evaluation of this term requires the following steps:

1. Compute the density matrix derivative with respect to the external electric field.
2. Compute the potential derivative once with respect to magnetic field (for the second term in the two sums) and once with respect to nuclear coordinates (for the first term).
3. Contract the set of charges ($\mathbf{q}$ and $\mathbf{q}^x$) with the other terms.
4. Sum up the QM/FQ and QM/PCM contributions.

8 Supporting Information

The Supporting Information is available free of charge on http://pubs.acs.org

Analytical/numerical intensities comparison for methyloxirane in water at incident wavelength of 532 nm.

Raman and ROA spectra of methyloxirane as a function of number of shapshots in the QM/FQ/PCM method.

References

(1) Tomasi, J.; Mennucci, B.; Cammi, R. Quantum Mechanical Continuum Solvation Models. *Chem. Rev.* **2005**, *105*, 2999–3093.

(2) Senn, H. M.; Thiel, W. QM/MM methods for biomolecular systems. *Angew. Chem. Int. Ed.* **2009**, *48*, 1198–1229.

(3) Cheeseman, J. R.; Shaik, M. S.; Popelier, P. L.; Blanch, E. W. Calculation of Raman optical activity spectra of methyl-β-d-glucose incorporating a full molecular dynamics simulation of hydration effects. *J. Am. Chem. Soc.* **2011**, *133*, 4991–4997.

(4) Mennucci, B. Modeling environment effects on spectroscopies through QM/classical models. *Phys. Chem. Chem. Phys.* **2013**, *15*, 6583–6594.

(5) Hopmann, K. H.; Ruud, K.; Pecul, M.; Kudelski, A.; Dračínský, M.; Bour, P. Explicit versus implicit solvent modeling of Raman optical activity spectra. *J. Phys. Chem. B* **2011**, *115*, 4128–4137.

(6) Cappelli, C.; Lipparini, F.; Bloino, J.; Barone, V. Towards an accurate description of anharmonic infrared spectra in solution within the polarizable continuum model: Reaction field, cavity field and nonequilibrium effects. *J. Chem. Phys.* **2011**, *135*, 104505.

(7) Egidi, F.; Giovannini, T.; Piccardo, M.; Bloino, J.; Cappelli, C.; Barone, V. Stereoelectronic, Vibrational, and Environmental Contributions to Polarizabilities of Large Molecular Systems: A Feasible Anharmonic Protocol. *J. Chem. Theory Comp.* **2014**, *10*, 2456–2464.

(8) Cappelli, C. Integrated QM/Polarizable MM/Continuum Approaches to Model Chiroptical Properties of Strongly Interacting Solute-Solvent Systems. *Int. J. Quant. Chem.* **2016**, *116*, 1532–1542.

(9) Lipparini, F.; Egidi, F.; Cappelli, C.; Barone, V. The Optical Rotation of Methyloxirane in Aqueous Solution: A Never Ending Story? *J. Chem. Theory Comput.* **2013**, *9*, 1880–1884.

(10) Warshel, A.; Levitt, M. Theoretical studies of enzymic reactions: dielectric, electrostatic and steric stabilization of the carbonium ion in the reaction of lysozyme. *J. Mol. Biol.* **1976**, *103*, 227–249.

(11) Field, M. J.; Bash, P. A.; Karplus, M. A combined quantum mechanical and molecular mechanical potential for molecular dynamics simulations. *J. Comput. Chem.* **1990**, *11*, 700–733.

(12) Gao, J. Hybrid quantum and molecular mechanical simulations: an alternative avenue to solvent effects in organic chemistry. *Acc. Chem. Res.* **1996**, *29*, 298–305.

(13) Friesner, R. A.; Guallar, V. Ab initio quantum chemical and mixed quantum mechanics/molecular mechanics (QM/MM) methods for studying enzymatic catalysis. *Annu. Rev. Phys. Chem.* **2005**, *56*, 389–427.

(14) Lin, H.; Truhlar, D. G. QM/MM: what have we learned, where are we, and where do we go from here? *Theor. Chem. Acc.* **2007**, *117*, 185–199.

(15) Monari, A.; Rivail, J.-L.; Assfeld, X. Theoretical modeling of large molecular systems. Advances in the local self consistent field method for mixed quantum mechanics/molecular mechanics calculations. *Acc. Chem. Res.* **2012**, *46*, 596–603.

(16) Mutter, S. T.; Zielinski, F.; Cheeseman, J. R.; Johannessen, C.; Popelier, P. L.; Blanch, E. W. Conformational dynamics of carbohydrates: Raman optical activity of D-glucuronic acid and N-acetyl-D-glucosamine using a combined molecular dynamics and quantum chemical approach. *Phys. Chem. Chem. Phys.* **2015**, *17*, 6016–6027.

(17) Zielinski, F.; Mutter, S. T.; Johannessen, C.; Blanch, E. W.; Popelier, P. L. The Raman optical activity of β-d-xylose: where experiment and computation meet. *Phys. Chem. Chem. Phys.* **2015**, *17*, 21799–21809.

(18) Yamamoto, S.; Kaminský, J.; Bouř, P. Structure and vibrational motion of insulin from Raman optical activity spectra. *Anal. Chem.* **2012**, *84*, 2440–2451.

(19) Day, P. N.; Jensen, J. H.; Gordon, M. S.; Webb, S. P.; Stevens, W. J.; Krauss, M.; Garmer, D.; Basch, H.; Cohen, D. An effective fragment method for modeling solvent effects in quantum mechanical calculations. *J. Chem. Phys.* **1996**, *105*, 1968–1986.

(20) Kairys, V.; Jensen, J. H. QM/MM boundaries across covalent bonds: a frozen localized molecular orbital-based approach for the effective fragment potential method. *J. Phys. Chem. A* **2000**, *104*, 6656–6665.

(21) Mao, Y.; Demerdash, O.; Head-Gordon, M.; Head-Gordon, T. Assessing Ion–Water Interactions in the AMOEBA Force Field Using Energy Decomposition Analysis of Electronic Structure Calculations. *J. Chem. Theory Comput.* **2016**, *12*, 5422–5437.

(22) Thole, B. T. Molecular polarizabilities calculated with a modified dipole interaction. *Chem. Phys.* **1981**, *59*, 341–350.

(23) Steindal, A. H.; Ruud, K.; Frediani, L.; Aidas, K.; Kongsted, J. Excitation energies in solution: the fully polarizable QM/MM/PCM method. *J. Phys. Chem. B* **2011**, *115*, 3027–3037.

(24) Jurinovich, S.; Curutchet, C.; Mennucci, B. The Fenna–Matthews–Olson Protein Revisited: A Fully Polarizable (TD) DFT/MM Description. *ChemPhysChem* **2014**, *15*, 3194–3204.

(25) Boulanger, E.; Thiel, W. Solvent boundary potentials for hybrid QM/MM computations

using classical drude oscillators: a fully polarizable model. *J. Chem. Theory Comput.* **2012**, *8*, 4527–4538.

(26) Rick, S. W.; Stuart, S. J.; Berne, B. J. Dynamical Fluctuating Charge Force Fields: Application to Liquid Water. *J. Chem. Phys.* **1994**, *101*, 6141–6156.

(27) Rick, S. W.; Berne, B. J. Dynamical Fluctuating Charge Force Fields: The Aqueous Solvation of Amides. *J. Am. Chem. Soc.* **1996**, *118*, 672–679.

(28) Egidi, F.; Russo, R.; Carnimeo, I.; D'Urso, A.; Mancini, G.; Cappelli, C. The Electronic Circular Dichroism of Nicotine in Aqueous Solution: A Test Case for Continuum and Mixed Explicit-Continuum Solvation Approaches. *J. Phys. Chem. A* **2015**, *119*, 5396–5404.

(29) Giovannini, T.; Olszówka, M.; Cappelli, C. Effective Fully Polarizable QM/MM Approach To Model Vibrational Circular Dichroism Spectra of Systems in Aqueous Solution. *J. Chem. Theory Comput.* **2016**, *12*, 5483–5492.

(30) Lipparini, F.; Cappelli, C.; Barone, V. A Gauge Invariant Multiscale Approach to Magnetic Spectroscopies in Condensed Phase: General Three-Layer Model, Computational Implementation and Pilot Applications. *J. Chem. Phys.* **2013**, *138*, 234108.

(31) Egidi, F.; Carnimeo, I.; Cappelli, C. The Optical Rotatory Dispersion of Methyloxirane in Aqueous Solution: Assessing the Performance of Density Functional Theory in Combination with a Fully Polarizable QM/MM/PCM Approach. *Opt. Mater. Express* **2015**, *5*, 196–209.

(32) Barron, L. D.; Buckingham, A. D. Rayleigh and Raman Scattering from Optically Active Molecules. *Mol. Phys.* **1971**, *20*, 1111–1119.

(33) Barron, L. D.; Bogaard, M. P.; Buckingham, A. D. Raman Scattering of Circularly Polarized Light by Optically Active Molecules. *J. Am. Chem. Soc.* **1973**, *95*, 603–605.

(34) Barron, L. D.; Bogaard, M. P.; Buckingham, A. D. Differential Raman Scattering of Right and Left Circularly Polarized Light by Asymmetric Molecules. *Nature* **1973**, *241*, 113–114.

(35) Polavarapu, P. L. Renaissance in chiroptical spectroscopic methods for molecular structure determination. *Chem. Rec.* **2007**, *7*, 125–136.

(36) Polavarapu, P. L. Ab Initio Vibrational Raman and Raman Optical Activity Spectra. *J. Phys. Chem.* **1990**, *94*, 8106–8112.

(37) Amos, R. D. Electric and magnetic properties of CO, HF, HCI, and CH3F. *Chem. Phys. Lett.* **1982**, *87*, 23–26.

(38) van Gisbergen, S. J. A.; Snijders, J. G.; Baerends, E. J. A Density Functional Theory Study of Frequency-Dependent Polarizabilities and Van der Waals Dispersion Coefficients for Polyatomic Molecules. *J. Chem. Phys.* **1995**, *103*, 9347–9354.

(39) Casida, M. E. In *Recent Advances in Density Functional Methods Part I*; Chong, D. P., Ed.; World Scientific, Singapore, 1995; pp 155–192.

(40) Liégeois, V.; Ruud, K.; Champagne, B. An Analytical Derivative Procedure for the Calculation of Vibrational Raman Optical Activity Spectra. *J. Chem. Phys.* **2007**, *127*, 204105.

(41) Ruud, K.; Thorvaldsen, A. J. Theoretical Approaches to the Calculation of Raman Optical Activity Spectra. *Chirality* **2009**, *21*, E54–E57.

(42) London, F. Théorie Quantique des Courants Interatomiques dans les Combinaisons Aromatiques. *J. Phys. Radium* **1937**, *8*, 397–409.

(43) Ditchfield, R. Self-consistent perturbation theory of diamagnetism. *Mol. Phys.* **1974**, *27*, 789–807.

(44) Cheeseman, J. R.; Frisch, M. J.; Devlin, F. J.; Stephens, P. J. Hartree-Fock and Density Functional Theory Ab Initio Calculation of Optical Rotation Using GIAOs: Basis Set Dependence. *J. Phys. Chem. A* **2000**, *104*, 1039–1046.

(45) Ruud, K.; Helgaker, T.; ; Bouř, P. Gauge-Origin Independent Density-Functional Theory Calculations of Vibrational Raman Optical Activity. *J. Phys. Chem. A* **2002**, *106*, 7448–7455.

(46) Ruud, K.; Helgaker, T. Optical Rotation Studied by Density-Functional and Coupled-Cluster Methods. *Chem. Phys. Lett.* **2002**, *352*, 533–539.

(47) Helgaker, T.; Ruud, K.; Bak, K. L.; Jørgensen, P.; Olsen, J. Vibrational Raman Optical Activity Calculations Using London Atomic Orbitals. *Faraday Discuss.* **1994**, *99*, 165–180.

(48) Kumata, Y.; Furukawa, J.; Fueno, T. The Effect of Solvents on the Optical Rotation of Propylene Oxide. *Bull. Chem. Soc. Jpn.* **1970**, *43*, 3920–3921.

(49) Wilson, S. M.; Wiberg, K. B.; Murphy, M. J.; Vaccaro, P. H. The Effects of Conformation and Solvation on Optical Rotation: Substituted Epoxides. *Chirality* **2008**, *20*, 357–369.

(50) Egidi, F.; Bloino, J.; Barone, V.; Cappelli, C. Toward an Accurate Modeling of Optical Rotation for Solvated Systems: Anharmonic Vibrational Contributions Coupled to the Polarizable Continuum Model. *J. Chem. Theory Comput.* **2012**, *8*, 585–597.

(51) Pecul, M.; Ruud, K. Ab Initio Calculation of Vibrational Raman Optical Activity. *Int. J. Quant. Chem.* **2005**, *104*, 816–829.

(52) Vidal, L. N.; Egidi, F.; Barone, V.; Cappelli, C. Origin Invariance in Vibrational Resonance Raman Optical Activity. *J. Chem. Phys.* **2015**, *142*, 174101.

(53) Lipparini, F.; Cappelli, C.; Barone, V. Linear response theory and electronic transition energies for a fully polarizable QM/classical hamiltonian. *J. Chem. Theory Comput.* **2012**, *8*, 4153–4165.

(54) Lipparini, F.; Cappelli, C.; Scalmani, G.; De Mitri, N.; Barone, V. Analytical first and second derivatives for a fully polarizable QM/classical hamiltonian. *J. Chem. Theory Comput.* **2012**, *8*, 4270–4278.

(55) Lipparini, F.; Cappelli, C.; Barone, V. A gauge invariant multiscale approach to magnetic spectroscopies in condensed phase: General three-layer model, computational implementation and pilot applications. *J. Chem. Phys.* **2013**, *138*, 234108.

(56) Lipparini, F.; Barone, V. Polarizable force fields and polarizable continuum model: A fluctuating charges/PCM approach. 1. theory and implementation. *J. Chem. Theory Comp.* **2011**, *7*, 3711–3724.

(57) Mortier, W. J.; van Genechten, K.; Gasteiger, J. Electronegativity Equalization: Application and Parametrization. *J. Am. Chem. Soc.* **1985**, *107*, 829–835.

(58) Chelli, R.; Procacci, P. A transferable polarizable electrostatic force field for molecular mechanics based on the chemical potential equalization principle. *J. Chem. Phys.* **2002**, *117*, 9175–9189.

(59) Sanderson, R. T. An Interpretation of Bond Lengths and a Classification of Bonds. *Science* **1951**, *114*, 670–672.

(60) Ohno, K. Some remarks on the Pariser-Parr-Pople method. *Theor. Chim. Acta* **1964**, *2*, 219–227.

(61) McWeeny, R. *Methods of molecular quantum mechanics*; Academic press: London, 1992.

(62) Barone, V.; Cossi, M. Quantum Calculation of Molecular Energies and Energy Gradients in Solution by a Conductor Solvent Model. *J. Phys. Chem. A* **1998**, *102*, 1995–2001.

(63) Cossi, M.; Rega, N.; Scalmani, G.; Barone, V. Energies, Structures, and Electronic Properties of Molecules in Solution with the C-PCM Solvation Model. *J. Comput. Chem.* **2003**, *24*, 669–681.

(64) Lipparini, F.; Scalmani, G.; Mennucci, B.; Frisch, M. J. Self-consistent field and polarizable continuum model: A new strategy of solution for the coupled equations. *J. Chem. Theory Comp.* **2011**, *7*, 610–617.

(65) Hecht, L.; Nafie, L. A. Theory of Natural Raman Optical Activity Part I. Complete Circular Polarization Formalism. *Mol. Phys.* **1991**, *72*, 441–469.

(66) Nafie, L. A. *Vibrational Optical Activity: Principles and Applications*; John Wiley & Sons Ltd.: Chichester, 2011.

(67) Quinet, O.; Champagne, B. Time-dependent Hartree–Fock schemes for analytical evaluation of the Raman intensities. *J. Chem. Phys.* **2001**, *115*, 6293–6299.

(68) Frisch, M.; Head-Gordon, M.; Pople, J. Direct analytic SCF second derivatives and electric field properties. *Chem. Phys.* **1990**, *141*, 189–196.

(69) Pulay, P. Second and third derivatives of variational energy expressions: Application to multiconfigurational self-consistent field wave functions. *J. Chem. Phys.* **1983**, *78*, 5043–5051.

(70) Amos, R. Calculation of polarizability derivatives using analytic gradient methods. *Chem. Phys. Lett.* **1986**, *124*, 376–381.

(71) Krykunov, M.; Autschbach, J. Calculation of Optical Rotation with Time-Periodic

Magnetic-Field-Dependent Basis Functions in Approximate Time-Dependent Density-Functional Theory. *J. Chem. Phys.* **2015**, *123*, 114103.

(72) Quinet, O.; Liégeois, V.; Champagne, B. TDHF evaluation of the dipole-quadrupole polarizability and its geometrical derivatives. *J. Chem. Theory Comp.* **2005**, *1*, 444–452.

(73) Besley, N. A.; Bryan, J. A. Partial Hessian Vibrational Analysis of Organic Molecules Adsorbed on Si(100). *J. Phys. Chem. C* **2008**, *112*, 4308–4314.

(74) Lipparini, F.; Cappelli, C.; Scalmani, G.; Mitri, N. D.; Barone, V. Analytical First and Second Derivatives for a Fully Polarizable QM/Classical Hamiltonian. *J. Chem. Theory Comput.* **2012**, *8*, 4270–4278.

(75) Abrahama, M. J.; Murtola, T.; Schulz, R.; Pálla, S.; Smith, J. C.; Hess, B.; Lindahl, E. GROMACS: High Performance Molecular Simulations through Multi-Level Parallelism from Laptops to Supercomputers. *SoftwareX* **2015**, *1-2*, 19–25.

(76) Mark, P.; Nilsson, L. Structure and dynamics of the TIP3P, SPC, and SPC/E water models at 298 K. *J. Phys. Chem. A* **2001**, *105*, 9954–9960.

(77) Neugebauer, J.; Reiher, M.; Kind, C.; Hess, B. A. Quantum chemical calculation of vibrational spectra of large molecules—Raman and IR spectra for buckminsterfullerene. *J. Comput. Chem.* **2002**, *23*, 895–910.

(78) Frisch, M. J.; Trucks, G. W.; Schlegel, H. B.; Scuseria, G. E.; Robb, M. A.; Cheeseman, J. R.; Scalmani, G.; Barone, V.; Petersson, G. A.; Nakatsuji, H.; Li, X.; Caricato, M.; Marenich, A. V.; Bloino, J.; Janesko, B. G.; Gomperts, R.; Mennucci, B.; Hratchian, H. P.; Ortiz, J. V.; Izmaylov, A. F.; Sonnenberg, J. L.; Williams-Young, D.; Ding, F.; Lipparini, F.; Egidi, F.; Goings, J.; Peng, B.; Petrone, A.; Henderson, T.; Ranasinghe, D.; Zakrzewski, V. G.; Gao, J.; Rega, N.; Zheng, G.; Liang, W.;

Hada, M.; Ehara, M.; Toyota, K.; Fukuda, R.; Hasegawa, J.; Ishida, M.; Nakajima, T.; Honda, Y.; Kitao, O.; Nakai, H.; Vreven, T.; Throssell, K.; Montgomery Jr., J. A.; Peralta, J. E.; Ogliaro, F.; Bearpark, M. J.; Heyd, J. J.; Brothers, E. N.; Kudin, K. N.; Staroverov, V. N.; Keith, T. A.; Kobayashi, R.; Normand, J.; Raghavachari, K.; Rendell, A. P.; Burant, J. C.; Iyengar, S. S.; Tomasi, J.; Cossi, M.; Millam, J. M.; Klene, M.; Adamo, C.; Cammi, R.; Ochterski, J. W.; Martin, R. L.; Morokuma, K.; Farkas, O.; Foresman, J. B.; Fox, D. J. Gaussian 16 Revision A.03. 2016; Gaussian Inc. Wallingford CT.

(79) Polavarapu, P. L.; Hecht, L.; Barron, L. D. Vibrational Raman Optical Activity in Substituted Oxiranes. *J. Phys. Chem.* **1993**, *97*, 1793–1799.

(80) Sebestík, J.; Bouř, P. Raman Optical Activity of Methyloxirane Gas and Liquid. *J. Phys. Chem. Lett.* **2011**, *2*, 498–502.

(81) Cammas, G.; Morssli, M.; Fabregue, E.; Bardet, L. Vibrational Spectra of Lactic Acid and Lactates. *J. Raman Spectrosc.* **1991**, *22*, 409–413.

(82) Qiu, S.; Li, G.; Wang, P.; Jia, G.; Feng, Z.; Li, C. Hydrogen Bonding in Homochiral Dimers of Hydroxyesters Studied by Raman Optical Activity Spectroscopy. *J. Raman Spectrosc.* **2012**, *43*, 503–513.

Graphical TOC Entry